American Mineralogist, Volume 76, pages 405–426, 1991

High-temperature electrical measurements and thermodynamic properties of Fe_3O_4-$FeCr_2O_4$-$MgCr_2O_4$-$FeAl_2O_4$ spinels

JOHAN NELL, BERNARD J. WOOD
Department of Geology, University of Bristol, Bristol BS8 1RJ, Great Britain

ABSTRACT

Electrical conductivity and thermopower measurements have been made on Fe_3O_4-$FeCr_2O_4$, Fe_3O_4-$MgCr_2O_4$, and Fe_3O_4-$FeCr_2O_4$-$FeAl_2O_4$ spinel solid solutions at 600 °C to 1400 °C and 1 atm. Our analysis of the data indicates that these are *n*-type small polaron conductors with, as in Fe_3O_4, electron hopping confined to the octahedral sites. If Cr^{3+} is not involved in the conduction mechanism (i.e., Fe^{2+}-Fe^{3+} hopping only) then, with octahedral site hopping, the combined thermopower-electrical conductivity technique enables high-temperature cation distributions to be obtained.

On the Fe_3O_4-$FeCr_2O_4$ join we have found, from measurements of the independent density of states, that hopping is octahedral and involves Fe^{2+} and Fe^{3+} only at compositions with 40% or more of Fe_3O_4, but that Cr^{3+} becomes involved in the conduction process at very $FeCr_2O_4$-rich compositions. We have therefore excluded data on very Cr-rich compositions, which also exhibit high activation energies, from our estimates of cation distributions.

The thermopower and electrical conductivity data were combined with earlier results on the joins Fe_3O_4-$MgFe_2O_4$, Fe_3O_4-$FeAl_2O_4$, and Fe_3O_4-$MgAl_2O_4$ to estimate cation distributions for compositions within the geologically important system (Mg^{2+},Fe^{2+})-$(Fe^{3+},Al^{3+},Cr^{3+})_2O_4$. The cation distributions were then combined with activity-composition relations and interphase partitioning data to derive a complete thermodynamic model for the complex system $(Mg^{2+},Fe^{2+})(Fe^{3+},Al^{3+},Cr^{3+})_2O_4$. The model, which takes explicit account of order-disorder relations, produces and successfully predicts a wide range of macroscopic thermodynamic measurements that have been made on simple and complex spinels. A computer program to generate cation distributions and activities is available from B. J. Wood.

INTRODUCTION

The importance of spinels as furnace smelting products and as petrogenetic indicators in a wide range of igneous and metamorphic rocks has been emphasized in many studies of their thermodynamic properties (e.g., Sack, 1982; Buddington and Lindsley, 1964; Irvine, 1965; Mattioli and Wood, 1988). We recently reported high-temperature thermopower and electrical conductivity measurements on Fe_3O_4-$MgFe_2O_4$, Fe_3O_4-$FeAl_2O_4$, and Fe_3O_4-$MgAl_2O_4$ spinel solid solutions (Nell et al., 1989) and used the results to estimate cation distributions from the model of Mason (1987). The cation distributions were subsequently combined with activity-composition relations and interphase partitioning data to develop an internally consistent thermodynamic model for $(Mg^{2+},Fe^{2+})(Fe^{3+},Al^{3+})_2O_4$ spinels (Nell and Wood, 1989). Application of the model to natural spinels is limited, however, since most geologically important systems contain Cr_2O_3 or TiO_2 components. We have therefore extended our electrical measurements to Cr_2O_3-bearing spinels in the system $(Mg^{2+},Fe^{2+})(Fe^{3+},Al^{3+},Cr^{3+})_2O_4$ which closely approximate the compositions of many naturally occurring members of the spinel group.

Characterization of order-disorder relations is central to the understanding of the thermodynamic properties of spinels (O'Neill and Navrotsky, 1983, 1984; Nell et al. 1989). In the system $(Mg^{2+},Fe^{2+})(Fe^{3+},Al^{3+},Cr^{3+})_2O_4$, Fe^{2+}, Mg^{2+}, and Al^{3+} disorder between tetrahedral and octahedral sites, whereas Cr^{3+}, by virtue of its size and crystal field stabilization, resides on octahedral sites only (O'Neill and Navrotsky, 1983, 1984). Although Cr^{3+} is ordered, its presence influences the partitioning of the other cations between octahedral and tetrahedral sites, as will be discussed further below. In this study, we report high-temperature thermopower and electrical conductivity data on Fe_3O_4-$FeCr_2O_4$, Fe_3O_4-$MgCr_2O_4$, and Fe_3O_4-$FeAl_2O_4$-$FeCr_2O_4$ solid solutions in an attempt to characterize high-temperature order-disorder relations in $(Mg^{2+},Fe^{2+})(Fe^{3+},Al^{3+},Cr^{3+})_2O_4$ solid solutions. Cation distributions determined from quenched samples are subject to great uncertainties because of reordering during quenching (O'Neill and Navrotsky, 1983) so that in situ, high-temperature measurements are required. These have been attempted for several spinel systems (e.g., Wu and Mason, 1981; Mason, 1987; Nell et al. 1989) by measuring thermopower and electrical conductivity and assum-

0003–004X/91/0304–0405$02.00

TABLE 1. Sample characterization

	$Fe^{2+}Fe^{3+}_{2x}Cr_{2-2x}O_4$			$Fe^{2+}_xMg_{1-x}Fe^{3+}_{2x}Cr_{2-2x}O_4$		
	$x = 0.25$	$x = 0.50$	$x = 0.75$	$x = 0.25$	$x = 0.50$	$x = 0.75$
FeO	31.72	31.54	31.69	9.65	17.60	25.14
Fe_2O_3*	18.51	35.91	52.10	19.85	38.62	55.55
	(1.02)	(0.76)	(0.68)	(0.30)	(0.40)	(0.56)
MgO	0.0	0.0	0.0	14.49	9.16	4.36
				(0.26)	(0.10)	(0.10)
Al_2O_3	0.68	0.32	0.19	0.50	0.39	0.36
	(0.02)	(0.02)	(0.05)	(0.14)	(0.02)	(0.02)
Cr_2O_3	48.60	32.53	17.05	55.32	34.67	16.45
	(0.48)	(0.24)	(0.40)	(0.70)	(0.32)	(0.30)
Total	99.51	100.30	101.03	99.81	100.44	101.86
No. of analyses**	5	5	5	5	5	6
$\frac{Fe^{2+}}{Fe^{2+} + Mg}$	1.0	1.0	1.0	0.272	0.519	0.764
$\frac{Fe^{3+}}{Fe^{3+} + Al + Cr}$	0.262	0.509	0.741	0.252	0.511	0.758
Cell edge	8.3997	8.3939	8.3844	8.3661	8.3841	8.3808
(Å)†	(2)	(3)	(5)	(3)	(5)	(4)
% density‡	92.0	93.6	95.5	87.3	91.0	90.7

	$Fe^{2+}Fe^{3+}_{2x}Al_{1-x}Cr_{1-x}O_4$			$Fe^{2+}Fe^{3+}_{2x}Al_{5/6(2-2x)}Cr_{1/6(2-2x)}O_4$		$Fe^{2+}Fe^{3+}_{2x}Al_{1/6(2-2x)}Cr_{5/6(2-2x)}O_4$	
	$x = 0.25$	$x = 0.50$	$x = 0.75$	$x = 0.25$	$x = 0.50$	$x = 0.25$	$x = 0.50$
FeO	34.71	33.53	32.40	37.11	35.01	32.74	32.76
Fe_2O_3*	19.50	38.33	53.95	20.63	39.02	18.71	36.81
	(0.89)	(0.34)	(0.58)	(0.39)	(0.45)	(0.45)	(0.55)
MgO	0.00	0.00	0.00	0.00	0.00	0.00	0.00
Al_2O_3	19.08	12.00	5.82	33.00	20.45	5.97	3.96
	(0.13)	(0.15)	(0.03)	(1.05)	(0.11)	(0.09)	(0.09)
Cr_2O_3	26.62	16.83	8.42	9.72	6.14	42.64	28.09
	(0.46)	(0.29)	(0.18)	(0.14)	(0.16)	(0.38)	(0.13)
Total	99.91	100.69	100.59	100.46	100.62	100.06	101.62
No. of analyses**	6	5	5	5	6	4	5
$\frac{Fe^{2+}}{Fe^{2+} + Mg}$	1.0	1.0	1.0	1.0	1.0	1.0	1.0
$\frac{Fe^{3+}}{Fe^{3+} + Al + Cr}$	0.252	0.512	0.750	0.250	0.504	0.257	0.507
Cell edge	8.3162	8.3398	8.3618	8.2556	8.3030	8.3729	8.3756
(Å)†	(4)	(6)	(7)	(5)	(3)	(5)	(15)
% density‡	89.0	87.5	92.4	89.0	87.4	90.0	91.2

Note:
* Fe_2O_3 calculated from stoichiometry. Standard deviations are for total Fe.
** $\pm 1\ \sigma$ values for each element are given in parentheses.
† Numbers in parentheses are $\pm 1\ \sigma$ for the final decimal place.
‡ Percentage of theoretical density.

ing that the spinels are *n*-type small polaron conductors with Fe^{2+}-Fe^{3+} electron hopping on octahedral sites only. The approach, in principle, should enable complete characterization of cation distributions over the entire range of compositions studied. We used the same method in our study with apparent success in some cases and in other cases more equivocal results. The data were then used, together with activity-composition measurements and interphase partitioning relations, to generate a complete thermodynamic model of $(Mg^{2+},Fe^{2+})(Fe^{3+},Al^{3+},Cr^{3+})_2O_4$ solid solutions.

Experimental methods

Solid solutions containing $x = 0.25$; 0.50 and 0.75 in $Fe^{2+}Fe^{3+}_{2x}Cr^{3+}_{(2-2x)}O_4$; $Fe^{2+}_xMg^{2+}_{(1-x)}Fe^{3+}_{2x}Cr^{3+}_{(2-2x)}O_4$; and $Fe^{2+}Fe^{3+}_{2x}Al^{3+}_{(1-x)}Cr^{3+}_{(1-x)}O_4$; as well as $x = 0.25$ and 0.50 in $Fe^{2+}Fe^{3+}_{2x}Al^{3+}_{5/6(2-2x)}Cr^{3+}_{1/6(2-2x)}O_4$ and $Fe^{2+}Fe^{3+}_{2x}Al^{3+}_{1/6(2-2x)}Cr^{3+}_{5/6(2-2x)}O_4$, were used for the electrical measurements. High-density polycrystalline samples were prepared from oxide starting mixes with repeated cycles of firing and grinding in a controlled gas atmosphere. Starting materials were reagent grade Fe_2O_3, Cr_2O_3, MgO, and Al_2O_3. The MgO and Al_2O_3 were obtained from the decarbonation and dehydration of $MgCO_3$ and $Al(OH)_3$ at 1200 °C, respectively. The Fe_2O_3 and Cr_2O_3 were dried at 400 °C. All oxides were stored in a desiccator.

Stoichiometric oxide mixtures were pressed into pellets and reacted at a temperature of 1300 °C in a vertical tube furnace through which a gas stream with a CO/CO_2 ratio of 0.3/100 was passed at a flow rate of approximately 1 linear cm/s ($\log P_{O_2} = -4.7$). Samples were reacted for 10 h at a time and, after 4 cycles of grinding and firing, single phase spinels were produced for every composition. Once prepared, the samples were crushed in a vi-

bratory mill (using alumina grinding medium) and isostatically cold pressed into pellets at a pressure of 2.75×10^8 Pa. The pellets were subsequently densified through sintering at 1300 °C under an atmosphere with $\log P_{O_2} = -4.7$ for 24 h. Final cell edges and percentages of the theoretical densities for each composition are reported in Table 1.

Thermopower (Q) and electrical conductivity (σ) measurements were conducted using a four-point measurement technique outlined by Nell et al. (1989). At all times, a gas mixture with a CO/CO_2 ratio of 0.3/100 was passed through the furnace at a flow rate of 1 linear cm/s. Measurements were made at 50–100 °C intervals, commencing at 1400 °C after 12 h of annealing to stabilize grain growth, down to approximately 600 °C and up again to 1400 °C. Values were recorded once thermal voltages were stable to ±1% over at least 30 min. Measurements taken in sequence from high to low T generally agreed with those recorded from low to high T, suggesting that equilibrium values were measured.

On the completion of the electrical measurements, the samples used for the measurements were mounted and polished for analysis by electron microprobe. Compositions are given in Table 1. Concentrations of Fe^{3+} have been calculated from stoichiometry. All the samples were chemically homogeneous single-phase spinel. No chemical zoning was observed and potential Fe depletion resulting from assimilation by thermocouple beads could not be detected. Most samples were slightly contaminated with Al_2O_3 derived from the alumina grinding medium used in the vibratory mill. The level of contamination rarely exceeds 1% by mass and is sufficiently low not to affect the electrical measurements.

Results

Thermopower (Q) results for the systems $Fe^{2+}Fe^{3+}_{2x}Cr^{3+}_{(2-2x)}O_4$, $Fe^{2+}_{x}Mg^{2+}_{(1-x)}Fe^{3+}_{2x}Cr^{3+}_{(2-2x)}O_4$, $Fe^{2+}Fe^{3+}_{2x}Al^{3+}_{(1-x)}Cr^{3+}_{(1-x)}O_4$, $Fe^{2+}Fe^{3+}_{2x}Al^{3+}_{1/6(2-2x)}Cr^{3+}_{5/6(2-2x)}O_4$, and $Fe^{2+}Fe^{3+}_{2x}Al^{3+}_{5/6(2-2x)}Cr^{3+}_{1/6(2-2x)}O_4$ are presented in Figures 1A, 2A, 3A, 4A, and 5A, respectively. Results obtained for Fe_3O_4 by Nell et al. (1989) are presented on each of the diagrams for comparison. Error bars on the data points correspond to a ±7% uncertainty in the absolute value of Q and represent an uncertainty of ±1 °C in the maximum temperature gradient for every measurement (Nell et al., 1989). Repeated heating and cooling cycles always produced the same result within experimental uncertainty and, in that sense, the data are reversible. In Fe_3O_4-$FeCr_2O_4$ and Fe_3O_4-$FeAl_2O_4$-$FeCr_2O_4$ solid solutions, there is a systematic decrease in the absolute value of thermopower with Fe_3O_4 dilution (Figs. 1A, 3A, 4A, and 5A). Given the assumption of octahedral Fe^{2+}-Fe^{3+} hopping, this decrease results from the substitution of Fe^{3+} by Cr^{3+} and Al^{3+}, which decreases the ratio Fe^{3+}/Fe^{2+} on octahedral sites. In Fe_3O_4-$MgCr_2O_4$, solid solutions Fe^{2+} and Fe^{3+} are replaced by Mg^{2+} and Cr^{3+}, respectively, and the ratio Fe^{3+}/Fe^{2+} on octahedral sites, as well as ther-

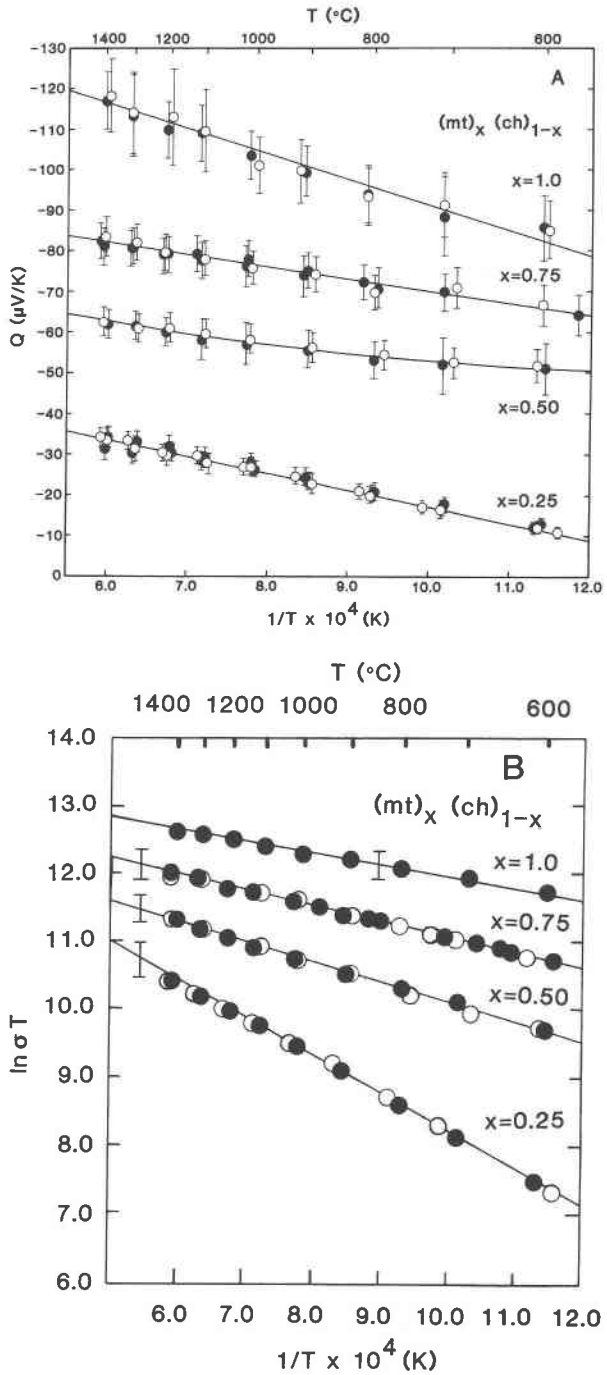

Fig. 1. (A) Thermopower measurements in the system Fe_3O_4 (mt)-$FeCr_2O_4$ (ch) as a function of temperature. Solid and open symbols in Figures 1–5 are down and up temperature measurements, respectively. Data for pure Fe_3O_4 in this and subsequent figures are from Nell et al. (1989). (B) Electrical conductivity data in Fe_3O_4-$FeCr_2O_4$ solid solutions as a function of temperature.

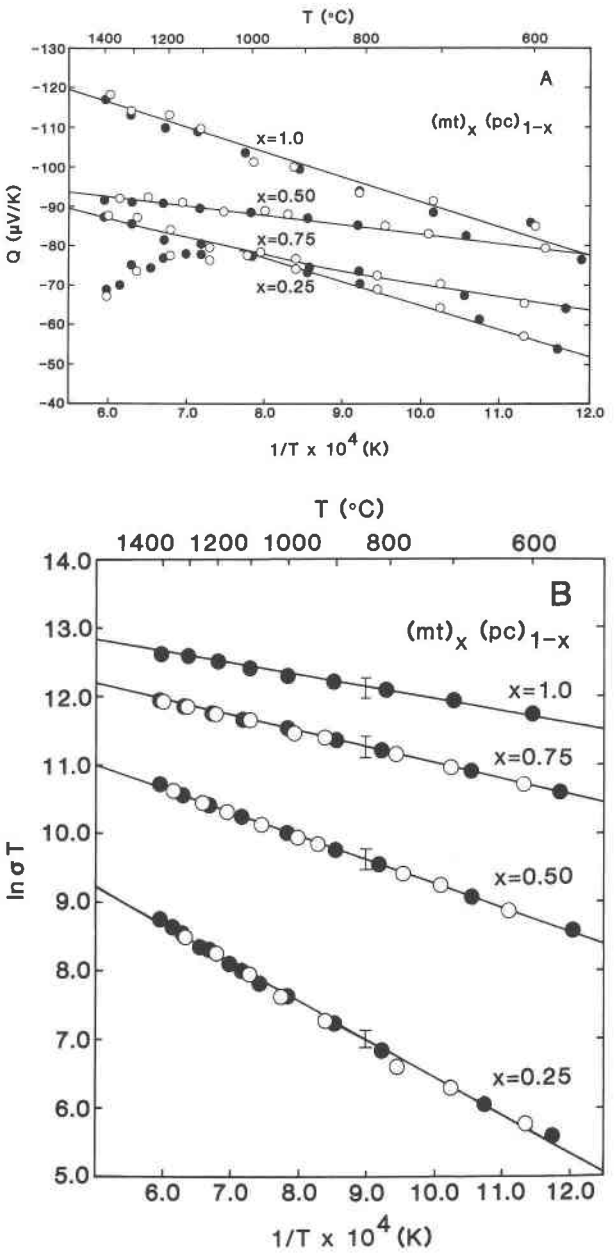

Fig. 2. (**A**) Thermopower measurements in Fe_3O_4 (mt)-$MgCr_2O_4$ (pc) solid solutions as a function of temperature. Notice the change in sign in the temperature derivative of Q at high temperatures in the sample $(mt)_{0.25}(pc)_{0.75}$. Error bars on the data have been omitted for clarity. Uncertainties are still, however, ±7% of the absolute value of Q. (**B**) Electrical conductivity measurements in Fe_3O_4-$MgCr_2O_4$ solid solutions as a function of temperature.

mopower, remains relatively constant throughout the compositional range investigated (Fig. 2A). Similar behavior has been observed in the system Fe_3O_4-$MgAl_2O_4$, where a comparable situation exists (Nell et al., 1989). The 25% sample Fe_3O_4-75% $MgCr_2O_4$ displays a reversal in the sign of the derivative of thermopower with respect to temperature at approximately 1050 °C (Fig. 2A). We consider it likely that this is caused by a change in the conduction mechanism between pure Fe_3O_4 and the $MgCr_2O_4$-rich end of the series.

Electrical conductivity (σ) data for $Fe^{2+}Fe^{3+}_{2x}Cr^{3+}_{(2-2x)}O_4$, $Fe^{2+}_xMg^{2+}_{(1-x)}Fe^{3+}_{2x}Cr^{3+}_{(2-2x)}O_4$, $Fe^{2+}Fe^{3+}_{2x}Al^{3+}_{(1-x)}Cr^{3+}_{(1-x)}O_4$, $Fe^{2+}Fe^{3+}_{2x}Al^{3+}_{1/6(2-2x)}Cr^{3+}_{5/6(2-2x)}O_4$, and $Fe^{2+}Fe^{3+}_{2x}Al^{3+}_{5/6(2-2x)}Cr^{3+}_{1/6(2-2x)}O_4$ solid solutions are in Figures 1B, 2B, 3B, 4B, and 5B, respectively. Conductivity data from Nell et al. (1989) are on each diagram for comparison. There is a general decrease in the conductivity of spinel solid solutions with magnetite dilution consistent with the expected decrease in the total number of conducting sites (Fe^{2+} + Fe^{3+}) present.

Thermopower and conductivity data were fit to the following polynomials:

$$Q = a + b(10^4/T) + c(10^4/T)^2 \qquad \mu V/K \qquad (1)$$

and

$$\ln \sigma T = A + B(10^4/T). \qquad (2)$$

The statistical significance of the second-degree term (c) in Equation 1 has been tested with the F-ratio and is only used for the compositions $Fe^{2+}Fe^{3+}Cr^{3+}O_4$ and $Fe^{2+}_{0.75}Mg^{2+}_{0.25}Fe^{3+}_{1.5}Cr^{3+}_{0.5}O_4$ where the confidence level for a quadratic relative to a linear relationship exceeds the 90% confidence level (Bevington, 1969, p. 200). It should be pointed out that, in the small polaron limit of a system with fixed carrier concentration, thermopower is independent of temperature. In Fe_3O_4 and Fe_3O_4 solid solutions, however, the carrier concentrations depend on temperature because of the disordering of Fe^{2+} and Fe^{3+} between octahedral and tetrahedral sites, and it is the temperature dependence of carrier concentration that is reflected by the polynomial to which thermopower has been fitted in Equation 1. The coefficients a, b, c, A, and B are reported in Table 2, and the resulting regression curves are presented as the solid lines in Figures 1–5. Error bars on the lines in Figures 1B, 2B, 3B, 4B, and 5B are ±15% of the mean values calculated from Equation 2 and represent the observed scatter in conductivity data.

The coefficient B in Equation 2 is proportional to the apparent activation energy (E_a)

$$B = \frac{-E_a \cdot e_o}{k \cdot 10^4} \qquad (3)$$

where k is Boltzmann's constant, e_o is the electronic charge, and E_a is the apparent hopping energy in eV obtained from the conductivity data when temperature and compositional dependencies of carrier concentrations are neglected ($\sigma = \exp[A - (E_a \cdot e_o/kT)]/T$). Values of E_a are reported in Table 2.

Electrical behavior and nonstoichiometry

In order to interpret our results, it is first necessary to be sure that the concentrations of the conducting species,

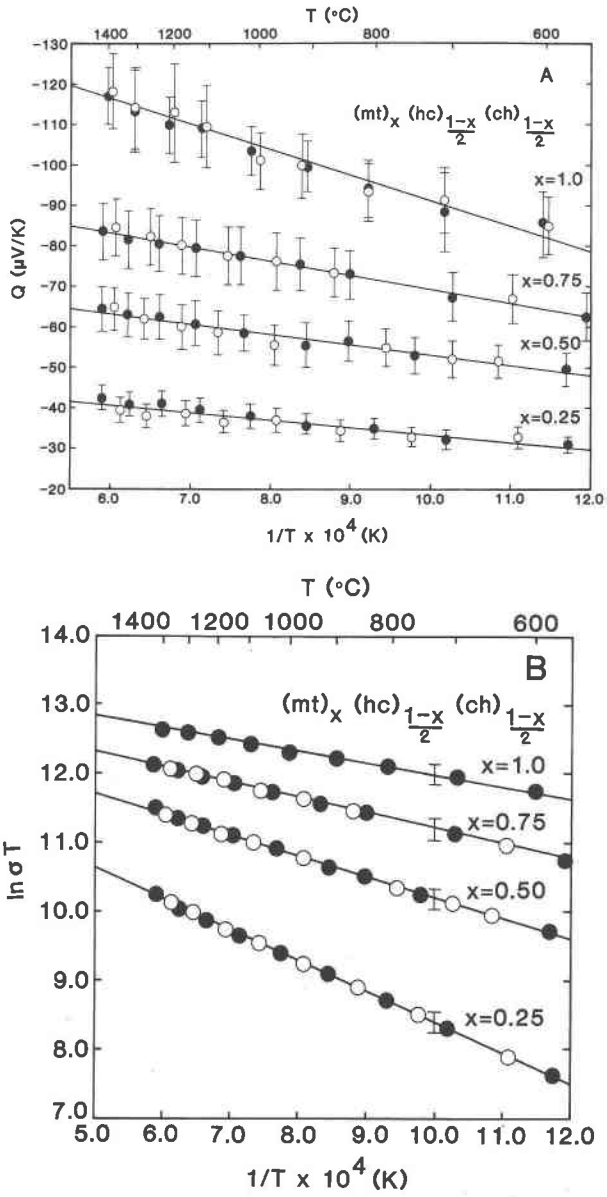

Fig. 3. (A) Thermopower measurements in Fe_3O_4 (mt)-$FeAl_2O_4$ (hc)-$FeCr_2O_4$ (ch) solid solutions measured along a pseudobinary section with the ratio of $FeCr_2O_4/(FeCr_2O_4 + FeAl_2O_4) = 1/2$. (B) Electrical conductivity data for the pseudobinary system $(mt)_x(hc)_{1/2(1-x)}(ch)_{1/2(1-x)}$.

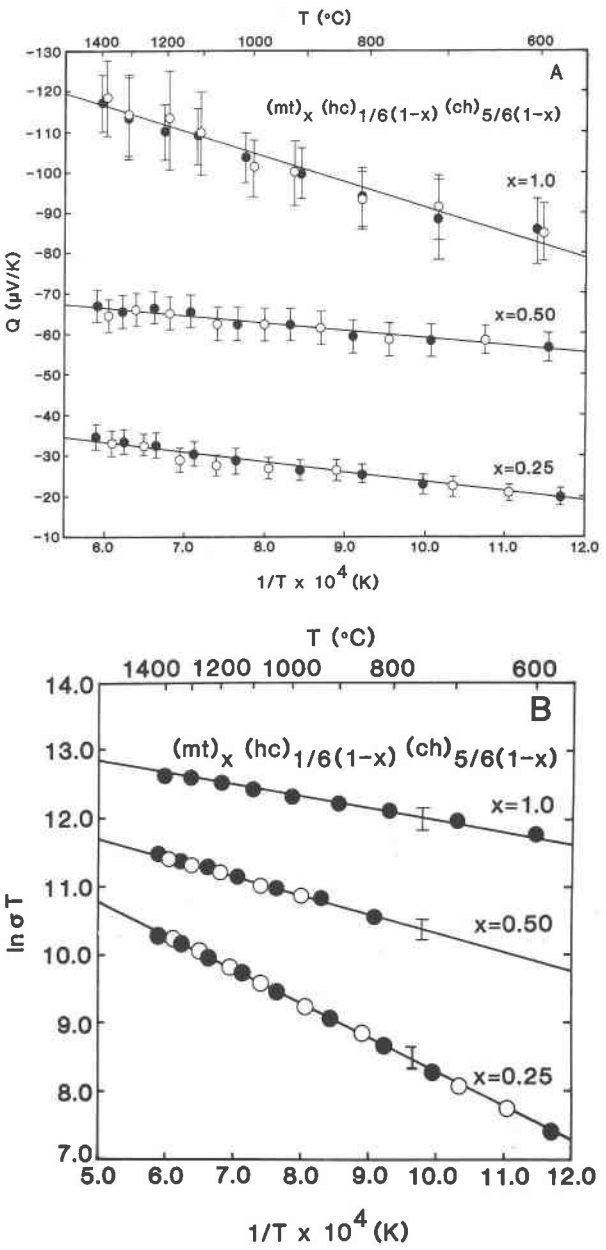

Fig. 4. (A) Thermopower results in Fe_3O_4-$FeAl_2O_4$-$FeCr_2O_4$ solid solutions measured along a pseudobinary section with the ratio of $FeCr_2O_4/(FeCr_2O_4 + FeAl_2O_4) = 5/6$. (B) Electrical conductivity data for the pseudobinary system $(mt)_x(hc)_{1/6(1-x)}$-$(ch)_{5/6(1-x)}$.

Fe^{2+} and Fe^{3+}, are known precisely. The total Fe content is, of course, known from the starting mixture and from microprobe analysis. The Fe^{2+}/Fe^{3+} ratios of single phase spinels depend on f_{O_2}, however, and we wished to maintain essentially the ideal spinel stoichiometry of three cations to four O atoms. Dieckmann (1982) has determined deviations from stoichiometry of pure Fe_3O_4, and, as a starting point, we applied his equations for magnetite to estimate the stoichiometry of our complex spinel solutions. The deviation from stoichiometry, δ [= (cation vacancies − Fe interstitials) per lattice molecule] (Dieckmann, 1982), is derived as follows:

$$\delta = \frac{(Fe^{2+}_{ss} - \delta)^3}{(Fe^{3+}_{ss} + 2\delta)^2} K_V (a_{O_2})^{2/3} (a^{ss}_{Fe_3O_4})^{-1/3} - \frac{(Fe^{3+}_{ss} + 2\delta)^2}{(Fe^{2+}_{ss} - \delta)^3} K_I (a_{O_2})^{-2/3} (a^{ss}_{Fe_3O_4})^{1/3} \quad (4)$$

where K_V is the vacancy equilibrium constant, K_I the

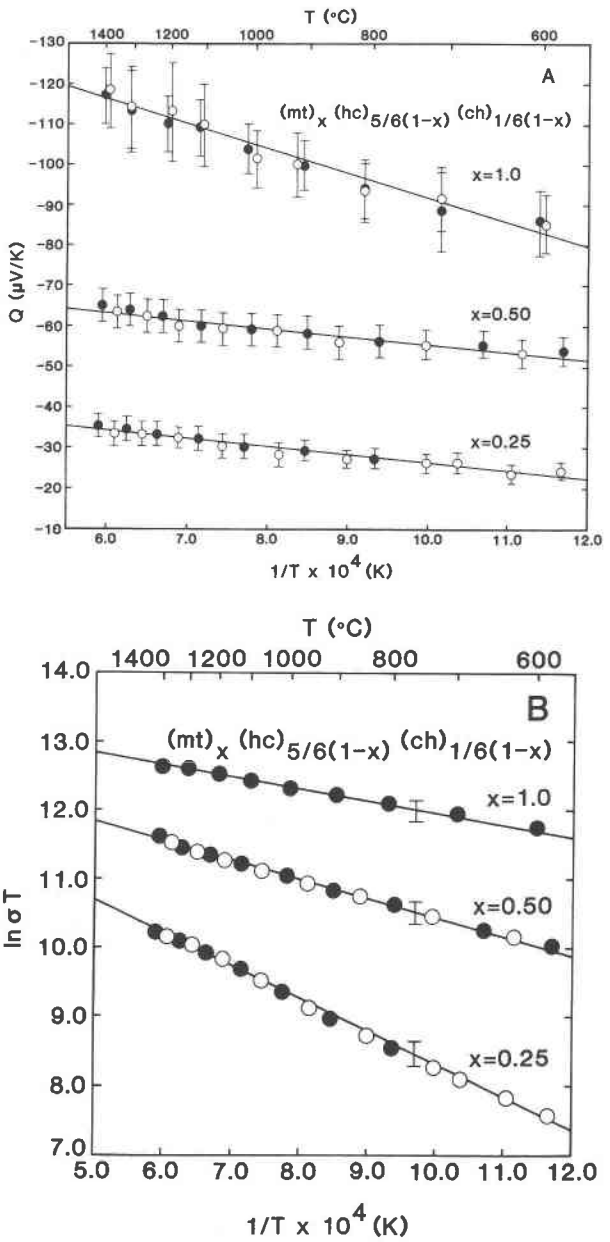

Fig. 5. (**A**) Thermopower measurements in Fe_3O_4-$FeAl_2O_4$-$FeCr_2O_4$ solid solutions measured along a pseudobinary section with the ratio of $FeCr_2O_4/(FeCr_2O_4 + FeAl_2O_4) = 1/6$. (**B**) Electrical conductivity data for the pseudobinary system $(mt)_x$-$(hc)_{5/6(1-x)}(ch)_{1/6(1-x)}$.

interstitial equilibrium constant, and the sub- and superscripts ss refer to the solid solution of interest. As an initial approximation, K_V and K_I were assumed to be independent of composition and the f_{O_2} at which δ equals zero were calculated using the equilibrium constants given by Dieckmann (1982) for pure magnetite. It was found that a CO/CO_2 ratio of approximately 0.3/100 would always yield f_{O_2} within about two log units of the P_{O_2} at which δ equals zero for the solid solution compositions of interest to us in this study. This should place the experiments in a plateau region of near zero deviation from stoichiometry (Dieckmann, 1982). The assumption of vacancy and interstitial equilibrium constants that are independent of composition is questionable, however. In order to assess the applicability of the approximation, we conducted thermopower and conductivity measurements on a dilute solid solution containing 25% Fe_3O_4 and 75% $MgAl_2O_4$ at 900 °C over a range of f_{O_2} of six log units. This composition and temperature was selected because of the availability of Fe_3O_4 activity data (Mattioli and Wood, 1988) and because it represents the most depleted magnetite concentrations examined in our study.

Thermopower and conductivity results are compared with the calculated defect concentration profile as a function of temperature in Figures 6A–6C, respectively. Thermopower follows the defect concentration profile closely while conductivity remains constant within uncertainty over the P_{O_2} range of our measurements (note that f_{O_2} more oxidizing than approximately 10^{-9} are difficult to achieve with CO-CO_2 mixtures at 900 °C). The pertinent observation is that there is, as in Fe_3O_4, a well-defined plateau in which both thermopower and electrical conductivity are insensitive to variations in P_{O_2}. This plateau extends over approximately five log units in f_{O_2} and corresponds to $|\delta| \leq 1 \times 10^{-3}$. The observed correspondence between thermopower and the calculated δ agrees with that expected for small polaron conduction in which Q depends on Fe^{3+}/Fe^{2+} (see Eq. 5 below). The correspondence between the calculated δ and thermopower suggests that neither K_V nor K_I varies greatly with composition, a condition also reported by Erickson and Mason (1985) for the Fe_3O_4-$CoFe_2O_4$ system.

In solid solutions where Fe^{3+} is replaced, but Fe^{2+} contents is unchanged, e.g., Fe_3O_4-$FeCr_2O_4$, the plateau region is displaced toward more reduced log P_{O_2} values by a factor of $\frac{2}{3}$ log $X_{Fe_3O_4}$ (Nell and Wood, unpublished data; Aragon and McCallister, 1982) if nonstoichiometry is associated only with the Fe_3O_4 component of the solid solution. The width of the plateau region should remain the same, however, at five log units in P_{O_2} at 900 °C. In a solid solution containing 25% Fe_3O_4 and 75% $FeCr_2O_4$, for example, the f_{O_2} at which δ equals zero at 900 °C is at log P_{O_2} equal to -12.6 while it is at -10.2 for a 25% Fe_3O_4–75% $MgAl_2O_4$ solid solution (Fig. 6C). This is to be compared with the values for pure Fe_3O_4 (log $P_{O_2} = -11.1$) and the gas mixture we used that gives a log P_{O_2} at 900 °C of -11.0. We conclude therefore that a gas mixture with a CO/CO_2 ratio of 0.3/100 should be in equilibrium with Fe_3O_4 solid solutions in which the deviation from stoichiometry is less than approximately 0.1% even when Fe_3O_4 content is diluted to 25%. As a check on this assumption, we always varied the gas composition slightly in solid solutions containing 25% Fe_3O_4 in order to test for fluctuations in the value of the thermoelectric coefficient that would serve as an indicator of deviations from stoichiometry approaching the shoulders of the plateau. None were observed. We consider, there-

fore, that our thermopower and conductivity data refer to stoichiometric spinels of the appropriate compositions, and that, in the region of interest, deviations from stoichiometry yield effects that are within experimental uncertainty (Figs. 6A, 6B). One of the reviewers also commented that the CO/CO_2 equilibrium is strongly temperature dependent and that use of a constant gas mixture could lead to f_{O_2} values not on the plateau at lower temperatures. The relations given by Dieckmann (1982) indicate, however, that curves of constant δ are essentially parallel to CO-CO_2 isopleths on a log P_{O_2} vs. temperature diagram, and that it is therefore appropriate to use a fixed gas mixture. We should also point out that our thermopower results for Fe_3O_4 (Nell et al., 1989), using a fixed gas composition, agree with the study of Wu and Mason (1981) in which great care was taken to preserve exact Fe_3O_4 stoichiometry over the temperature range 600–1500 °C.

Thermopower and conductivity theory

Electrical conductivity and thermopower measurements on spinels, although of some inherent mineralogical interest, are of most value if they can be used to cast light on the distribution of charge carriers in the crystal structure. This requires a correct interpretation of the conductivity mechanism, something that is difficult to do meaningfully in these complex phases. However, in the temperature range of our study (600–1400 °C), the measured activation energy of approximately 0.12 eV for electrical conduction in magnetite coupled with the low carrier mobility has been used by many authors to infer a small polaron mechanism. This will be discussed in more detail below.

We begin, however, with a brief review of conduction behavior in Fe_3O_4 at low temperature, where the results are more ambiguous. Kuipers and Brabers (1979) observed thermally activated drift mobilities above and be-

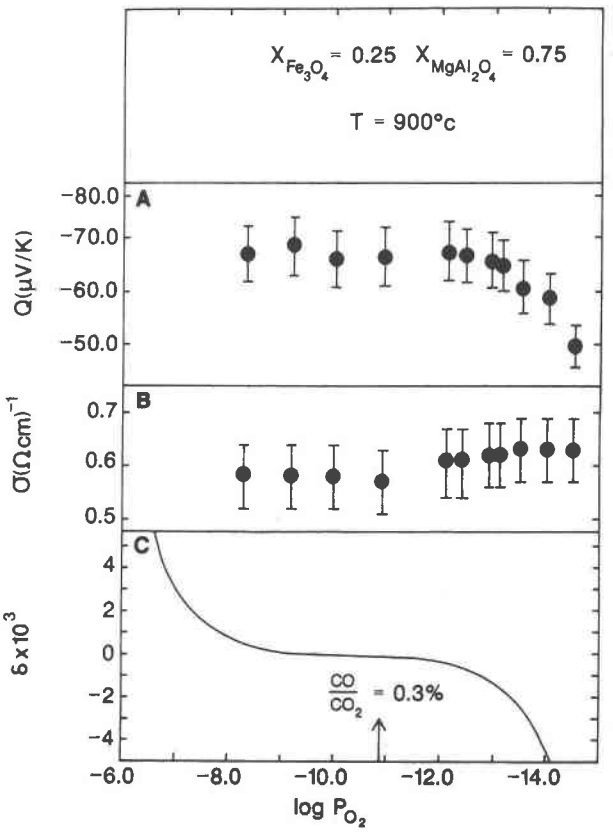

Fig. 6. (A) Thermopower measurements in a solid solution containing 25% Fe_3O_4 and 75% $MgAl_2O_4$ at 900 °C as a function of log P_{O_2}. (B) Electrical conductivity measurements in $Mg_{0.75}Fe_{0.75}Al_{1.5}O_4$ as a function of log P_{O_2}. (C) Defect profile for $Mg_{0.75}Fe_{0.75}Al_{1.5}O_4$ as a function of log P_{O_2}.

Table 2. Polynomial fit parameters for the thermopower and conductivity data sets

System	$Fe^{2+}Fe^{3+}_{2x}Cr_{2-2x}O_4$			$Fe^{2+}_xMg_{1-x}Fe^{3+}_{2x}Cr_{2-2x}O_4$		
Composition	$x = 0.25$	$x = 0.50$	$x = 0.75$	$x = 0.25$	$x = 0.50$	$x = 0.75$
Coefficients						
a	−58.1	−91.9	−100.0	−124.0	−106.9	−124.5
b	4.1	6.3	3.0	5.9	2.4	7.4
c	0.0	−0.2	0.0	0.0	0.0	−0.2
A	13.742	13.081	13.389	12.002	12.708	13.306
B	−0.547	−0.296	−0.227	−0.554	−0.345	−0.228
E_a (eV)	0.47	0.255	0.20	0.48	0.30	0.19

System	$Fe^{2+}Fe^{3+}_{2x}Al_{1-x}Cr_{1-x}O_4$			$Fe^{2+}Fe^{3+}_{2x}Al_{5/6(2-2x)}Cr_{1/6(2-2x)}O_4$		$Fe^{2+}Fe^{3+}_{2x}Al_{1/6(2-2x)}Cr_{5/6(2-2x)}O_4$	
Composition	$x = 0.25$	$x = 0.50$	$x = 0.75$	$x = 0.25$	$x = 0.50$	$x = 0.25$	$x = 0.50$
Coefficients							
a	−51.7	−78.2	−103.8	−46.1	−74.5	−48.0	−77.9
b	1.8	2.5	3.4	1.9	1.9	2.5	1.9
c	0.0	0.0	0.0	0.0	0.0	0.0	0.0
A	12.868	13.278	13.440	13.094	13.278	13.323	13.158
B	−0.447	−0.307	−0.223	−0.478	−0.286	−0.507	−0.285
E_a (eV)	0.38	0.26	0.19	0.41	0.25	0.48	0.25

low the Verwey transition (~120 K) and ascribed conduction to phonon-assisted tunnelling or hopping possibly caused by small polaron formation. Chakraverty (1980), on the other hand, proposed bipolaron formation as a result of ordering between neighboring Fe^{2+}-Fe^{2+} pairs, whereas Ihle and Lorenz (1986) interpreted the electrical conductivity in terms of the superposition of small polaron band and small polaron hopping conduction. They noted however that, above 350 K, the small polaron band conduction decreases rapidly in favor of the hopping mechanism. Aragon and Honig (1988) found that the main features of the electrical conductivity and thermoelectric power measurements at temperatures above and below the Verwey transition can be described with a small polaron model when the thermal dependence of the density of states is taken into account. Other mechanisms that have been proposed include intermediate polaron formation with long-range ordered Fe^{2+}-Fe^{3+} pairs being responsible for conduction and charge density waves where itinerant electrons are the charge carriers (Goodenough, 1980). Following this analysis, Ghose (1988) also considered the possibility of intermediate polaron formation at low temperatures in his discussion of the electrical conduction of ilvaite. At temperatures above 310 K, however, the gradual loss of long-range order destroys the Fe^{2+}-Fe^{3+} pairs, and at temperatures above 405 K, all long-range order is lost and conduction is dominated by small polaron hopping.

Most of the possible low-temperature conduction mechanisms are excluded at the high temperatures (600–1400 °C) at which our experiments were conducted. The loss of long- and short-range Fe^{3+}-Fe^{2+} and Fe^{2+}-Fe^{2+} order with increasing temperature argues against the presence of intermediate polarons and bipolarons, respectively; whereas, itinerant electron conduction is inconsistent with the small activated drift mobilities observed for magnetite (Dieckmann et al., 1983) and magnetite solid solutions at high temperatures (e.g., Nell et al., 1989). The transition temperature from band type behavior (see below) to hopping motion for small polarons has been estimated to be approximately $\theta/2$ where θ is the Debye temperature (Austin and Mott, 1969). This agrees with the result of Ihle and Lorenz (1986) that conduction resulting from hopping dominates in Fe_3O_4 above 350 K given that θ for Fe_3O_4 is approximately 605 K (Grønvold and Sveen, 1974). Small polaron hopping should therefore dominate in the temperature range of our study, a conclusion reached on the basis of the moderate activation energy and low drift mobility observed by Verwey et al. (1947), Tannhauser (1962), Dieckmann et al. (1983), and Mason and Bowen (1981), among others. The remaining question, however, is whether electron hopping takes place between octahedral sites only, between tetrahedral sites only, or involves both types of sites.

In a study of intervalence charge transfer in silicates, Amthauer and Rossman (1984) found that small polaron hopping between Fe^{2+} and Fe^{3+} only occurs if these ions occupy equivalent or geometrically similar nearest-neighbor sites that share common edges or faces to form infinite chains, sheets, or three-dimensional networks. This observation was explained by the molecular orbital calculations of Sherman (1987) who investigated several mixed valence Fe-O clusters with edge-sharing cation polyhedra. In the case of Fe^{2+} and Fe^{3+} octahedra sharing an edge, the t_{2g} atomic orbitals of the two ions overlap to some extent, giving partial metal-metal bonding thereby facilitating electron transfer. In the spinel structure, octahedral sites form infinite edge-sharing networks with one another, but share corners with tetrahedral sites. The tetrahedral sites are isolated from one another. Therefore in spinel, octahedral-octahedral electron hopping is favored over octahedral-tetrahedral or tetrahedral-tetrahedral transfer.

High-temperature electrical conductivity data for Fe_3O_4 were correlated with the product of the concentrations of Fe^{2+} and Fe^{3+} on octahedral sites only by Tannhauser (1962), Dieckmann et al. (1983), and Mason and Bowen (1981) while Verwey et al. (1947) and Bannerjee et al. (1967) also interpreted their conductivity results in terms of electron hopping on octahedral sites based on the assumption (now known to be a poor approximation) of inverse cation distributions at high temperatures. In all studies, the hopping energy was found to be approximately 0.12 eV. Independent evidence for electron hopping between octahedral sites in magnetite has been provided by Mössbauer studies where absorption ascribed to $Fe^{2.5+}$ on the octahedral sites is observed (e.g., Kündig and Hargrove, 1969). Thermally activated electron hopping on octahedral sites was also observed by Lotgering and Van Diepen (1977) in a Mössbauer study of Zn-Ti ferrites between 78 K and 300 K. We infer therefore that experimental and theoretical evidence is heavily in favor of octahedral hopping in pure Fe_3O_4 and presumably also in ferrites close to magnetite in composition.

The assumption of electron hopping on octahedral sites only enabled Wu and Mason (1981) to estimate the partitioning of Fe^{2+} and Fe^{3+} between octahedral and tetrahedral sites in magnetite from their measurements of the thermoelectric coefficient. Given that there is no local Fe^{2+}-Fe^{3+} order in the structure and that electron-electron repulsion is sufficiently large to prevent double occupancy of a given site, the thermoelectric coefficient (Q) for an n-type small polaron conductor is given by

$$Q = -\frac{k}{e_o}\left\{\ln\left[2\left(\frac{[6]Fe^{3+}}{[6]Fe^{2+}}\right)\right] + A\right\} \quad V/K \qquad (5)$$

(Chaikin and Beni, 1976; Wu and Mason, 1981; Austin and Mott, 1969) where k is Boltzmann's constant, e_o is the electronic charge, and A is the vibrational entropy associated with the ions surrounding a polaron on a given site. If conduction takes place in systems where the conducting sites all have approximately the same energy (e.g., the octahedral spinel sublattice) A is assumed to be negligibly small (Austin and Mott, 1969; Emin, 1975). From Equation 5 it is clear that the thermoelectric coefficient

directly gives the ratio (Fe^{3+}/Fe^{2+}) on octahedral sites, provided the conditions of disorder and single occupation are fulfilled. In that case Q is sufficient to fully characterize cation distributions in Fe_3O_4 and in solid solutions such as Fe_3O_4-$FeCr_2O_4$ where only Fe^{2+} and Fe^{3+} are disordered between octahedral and tetrahedral sites. Wu and Mason (1981) measured the thermoelectric coefficient of magnetite at high temperature and, based on the assumption of octahedral site electron hopping, showed that the Fe^{2+}-Fe^{3+} distribution changes as anticipated from almost completely inverse (low $^{[6]}Fe^{3+}/^{[6]}Fe^{2+}$) at low temperatures to essentially completely disordered at temperatures close to 1500 °C. As Fe_3O_4 is diluted by other components, the same conduction mechanism should apply at least over limited ranges of solid solution, enabling cation distributions to be determined in more complex spinels. In Fe_3O_4-$MgCr_2O_4$ and Fe_3O_4-$FeAl_2O_4$-$FeCr_2O_4$ solid solutions, however, three cations (Fe^{2+}, Fe^{3+}, Mg^{2+} and Fe^{2+}, Fe^{3+}, Al^{3+}, respectively) are disordered and additional information is required to derive the intersite cation distributions. In these cases, measurement of the electrical conductivity (σ) provides the required data if the conduction mechanism is unchanged.

In the adiabatic limit of small polaron transport, the probability that an electron will respond rapidly enough to a coincidence event to execute a successful hop is approximately equal to 1 (Holstein, 1959; Tuller and Nowick, 1977), and the electrical conductivity for the small polaron conductor in this limit is given by

$$\sigma = \frac{Nc'(1 - c')ga^2e^2\nu_o}{kT} \exp\left(\frac{-E_H}{kT}\right) \quad (\Omega cm)^{-1} \qquad (6)$$

(Tuller and Nowick, 1977; Dieckmann et al., 1983), where g is a geometric factor that is constant for a given system, a is the jump distance (cm), ν_o is the lattice vibration frequency, N is the density of conducting sites (cm^{-3}), c' is the fraction of conducting sites occupied by charge carriers, $(1 - c')$ is the fraction of available jump sites, E_H is the hopping energy, and the remaining terms have their usual meaning. In the case of spinels with electron hopping on octahedral sites only, $c' = {}^{[6]}Fe^{2+}/({}^{[6]}Fe^{2+} + {}^{[6]}Fe^{3+})$, $(1 - c') = {}^{[6]}Fe^{3+}/({}^{[6]}Fe^{2+} + {}^{[6]}Fe^{3+})$, and N becomes the total concentration ${}^{[6]}Fe^{2+} + {}^{[6]}Fe^{3+}$. By normalizing the electrical conductivity of a mixed spinel to that of pure Fe_3O_4 ($N = 2.0$), the total concentration of ${}^{[6]}Fe^{2+} + {}^{[6]}Fe^{3+}$ can be calculated for the composition of interest (Mason, 1987; Nell et al., 1989). Measurement of ${}^{[6]}Fe^{3+}/{}^{[6]}Fe^{2+}$ and ${}^{[6]}Fe^{2+} + {}^{[6]}Fe^{3+}$ allows complete calculation of cation distributions in Fe_3O_4-$MgCr_2O_4$ and Fe_3O_4-$FeAl_2O_4$-$FeCr_2O_4$ solid solutions.

In our previous work (Nell et al., 1989) on the joins Fe_3O_4-$MgFe_2O_4$, Fe_3O_4-$FeAl_2O_4$, and Fe_3O_4-$MgAl_2O_4$, we found that dilution of Fe_3O_4 with the additional components brought changes in Q and σ which are consistent with the conduction mechanism remaining unchanged from $X_{Fe_3O_4}$ of 1.0 down to at least 0.25. By assuming that only octahedral hopping occurs and using Equations 5 and 6, we obtained cation site occupancies and activation energies that varied monotonically with composition. Furthermore, partitioning of Fe^{2+} and Fe^{3+} between octahedral and tetrahedral sites was found to closely obey the spinel model of O'Neill and Navrotsky (1983, 1984), which was derived from a wide variety of data on a large number of unary and binary spinels. Our results are therefore consistent with octahedral hopping only of Fe^{2+}-Fe^{3+} in these systems.

Although octahedral hopping appears to dominate in spinels, application of Equations 5 and 6 may still become invalid if other electron donors or acceptors, such as Cr^{3+} or Ti^{4+}, are present and involved in conduction. Bannerjee et al. (1967) and Verwey et al. (1947), for example, found evidence for a transition from octahedral site electron hopping between Fe^{2+} and Fe^{3+} to a different type of conduction mechanism with increasing magnetite dilution in the systems Fe_3O_4-Fe_2TiO_4 and Fe_3O_4-$MgCr_2O_4$, respectively. In both systems, inflection points in plots of the activation energy of hopping vs. composition indicate a transition from hopping of Fe^{2+}-Fe^{3+} between octahedral sites (activation energies of approximately 0.15 to 0.25 eV) to a different type of conduction mechanism (activation energies of approximately 0.4–0.5 eV). In view of the large energy barriers expected for tetrahedral and mixed site electron hopping, the observed second conduction mechanisms can probably be attributed to electron hopping between Fe^{2+} and Ti^{4+} and Fe^{2+} and Cr^{3+}, respectively (D. Sherman, personal communication). Large compositional dependencies of activation energy are not, however, observed in any of the systems in which Fe^{2+} and Fe^{3+} are diluted by Mg^{2+} and Al^{3+} (Nell et al., 1989), presumably because neither of the latter ions can contribute to conduction.

Our data support the suggestion that Cr^{3+} becomes involved in the electron hopping process. Figure 7 shows activation energy as a function of composition for the join Fe_3O_4-$FeCr_2O_4$. In the $FeCr_2O_4$-rich region of the join ($X_{FeCr_2O_4} \geq 0.75$), activation energies for conduction are constant at approximately 0.5 eV. In more Fe_3O_4-rich compositions, activation energy increases monotonically from 0.13 eV to 0.25 eV with increasing $FeCr_2O_4$ content. There appears to be a region of rapidly increasing activation energy between 0.6 and 0.75 $X_{FeCr_2O_4}$. Our provisional interpretation of the data was that in the region $0 \leq X_{FeCr_2O_4} \leq 0.6$, conduction is by octahedral hopping between Fe^{2+} and Fe^{3+} only, whereas the more Cr-rich compositions exhibit mixed Fe^{2+}-Fe^{3+}-Cr^{3+} electron transfer. As a test of this hypothesis, we applied Equations 5 and 6 to the values of thermopower and electrical conductivity of Fe_3O_4-$FeCr_2O_4$ solid solutions. In this case, if octahedral hopping between Fe^{2+} and Fe^{3+} is the sole mechanism, then with Cr present only on octahedral sites, Equations 5 and 6 enable us to calculate N, the densities of conducting ($Fe^{2+} + Fe^{3+}$) sites and to compare them with the expected values of 1.5, 1.0, and 0.5 for 75, 50, and 25 mol% Fe_3O_4, respectively. The data reveal excellent agreement between calculated and nominal N values

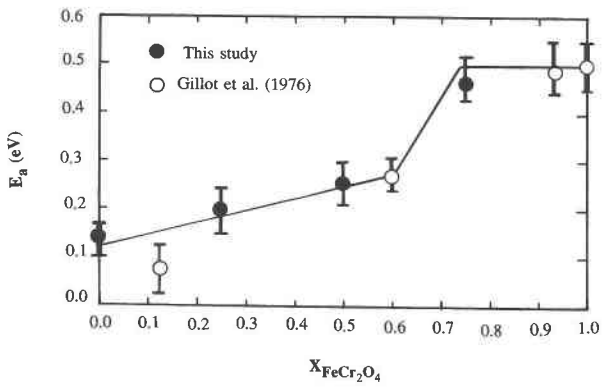

Fig. 7. Apparent hopping energies in the system Fe_3O_4-$FeCr_2O_4$ as a function of composition.

over the entire temperature range 600 °C to 1400 °C for solid solutions containing 75 and 50% Fe_3O_4. For the composition containing 25 mol% Fe_3O_4 however, the data give physically impossible values requiring a change in conduction mechanism. We conclude therefore that octahedral Fe^{2+}-Fe^{3+} hopping almost certainly occurs at Fe_3O_4 concentrations to 40% on this join but not at more $FeCr_2O_4$-rich compositions. We also consider that inflection points in plots of activation energy vs. composition (Fig. 7) are likely wherever there is a change in the conduction mechanism. Such inflections in activation energy were found in the binaries Fe_3O_4-$FeCr_2O_4$ and Fe_3O_4-$MgCr_2O_4$ and for two joins we studied in the Fe_3O_4-$FeAl_2O_4$-$FeCr_2O_4$ ternary (Table 2). In the case of $MgCr_2O_4$, unusual thermopower results were also observed in the 25% Fe_3O_4 composition (Fig. 2A).

In conclusion, we should state that we are unable to prove conclusively that octahedral Fe^{2+}-Fe^{3+} hopping is the sole mechanism operating in the complex spinels we have studied. The experimental and theoretical evidence in favor of its operating in pure Fe_3O_4 is, however, overwhelming. Furthermore, conductivity results on the joins Fe_3O_4-$FeAl_2O_4$, Fe_3O_4-$MgFe_2O_4$, and Fe_3O_4-$MgAl_2O_4$ exhibit only small increases in activation energy with Fe_3O_4 dilution, and calculated cation distributions are crystallographically reasonable. On the Fe_3O_4-$FeCr_2O_4$ join, the assumption of Fe^{2+}-Fe^{3+} hopping gives the correct concentration of (Fe^{2+} + Fe^{3+}) on octahedral sites at up to 50% $FeCr_2O_4$ substitution, confirming octahedral Fe^{2+}-Fe^{3+} hopping. Changes in conduction mechanism have also been recognized by sharp increases in activation energy and independently confirmed on the Fe_3O_4-$FeCr_2O_4$ join from the density of states calculations. We therefore believe that, after excluding data at 75% Cr^{3+} substitution for Fe^{3+}, we are justified in using Equations 5 and 6 to estimate cation distributions in these complex spinels.

Cation distributions

Cation distributions in Fe_3O_4-$FeCr_2O_4$, Fe_3O_4-$MgCr_2O_4$, and Fe_3O_4-$FeAl_2O_4$-$FeCr_2O_4$ solid solutions were

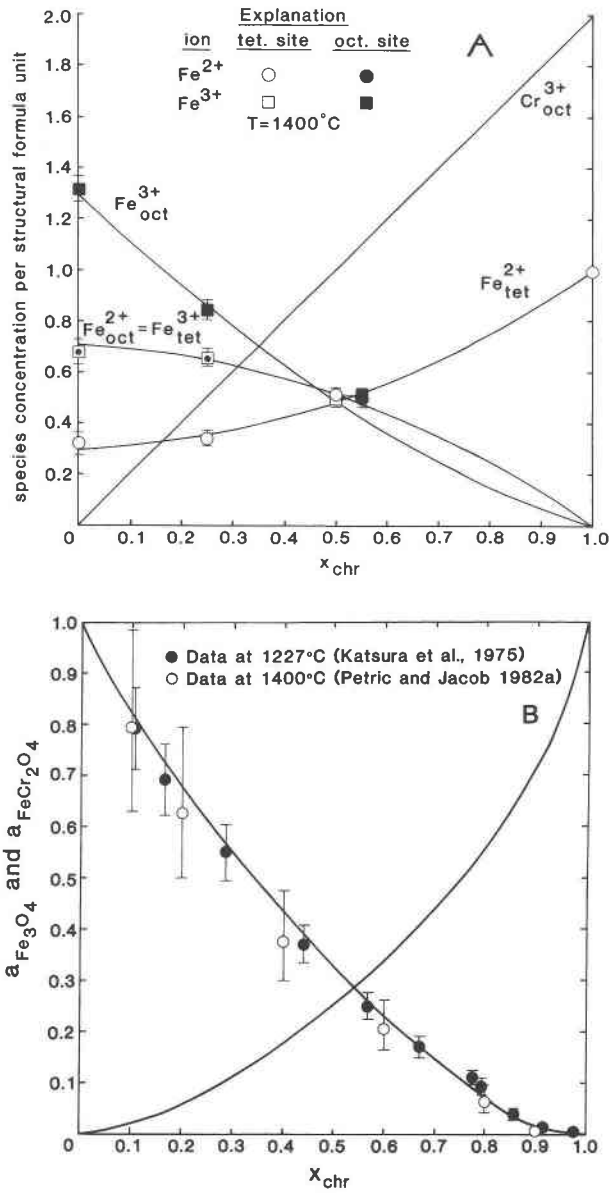

Fig. 8. (**A**) Cation distributions on the join Fe_3O_4-$FeCr_2O_4$ at 1400 °C plotted as a function of $FeCr_2O_4$ mole fraction (X_{chr}). Solid curves are distributions calculated from the model (see text). (**B**) Activity-composition relations in Fe_3O_4-$FeCr_2O_4$ solid solutions calculated at 1227 °C. Also shown are data from Katsura et al. (1975) at 1227 °C and Petric and Jacob (1982a) at 1400 °C.

calculated from the mass-balance, charge-balance, and stoichiometry conditions listed in Table 3. At fixed mole fraction (x) of Fe_3O_4 in Fe_3O_4-$FeCr_2O_4$ solid solutions, only the thermoelectric coefficient is required to determine cation distributions since $N = {}^{[6]}Fe^{2+} + {}^{[6]}Fe^{3+} = 2X_{Fe_3O_4}$. In Fe_3O_4-$MgCr_2O_4$ and Fe_3O_4-$FeAl_2O_4$-$FeCr_2O_4$ solid solutions, N was calculated from electrical conductivity measurements (Nell et al., 1989; Mason, 1987), which then allowed calculation of cation distributions

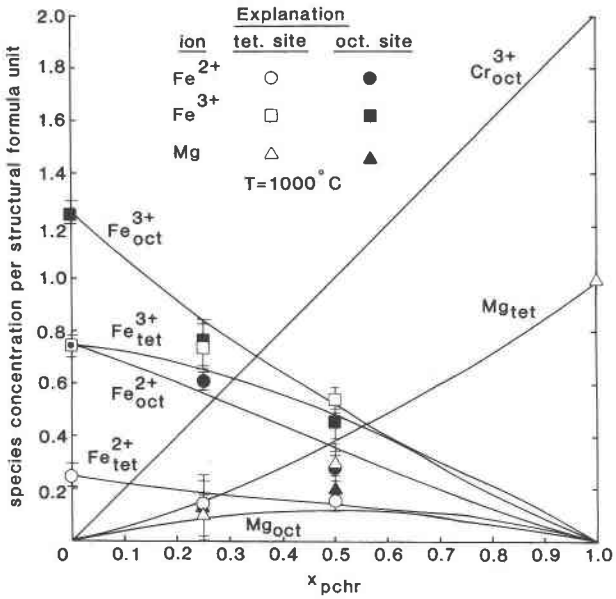

Fig. 9. Cation distributions on the join Fe_3O_4-$MgCr_2O_4$ at 1000 °C plotted as a function of mole fraction $MgCr_2O_4$ (X_{pchr}). Solid curves are distributions calculated from the model.

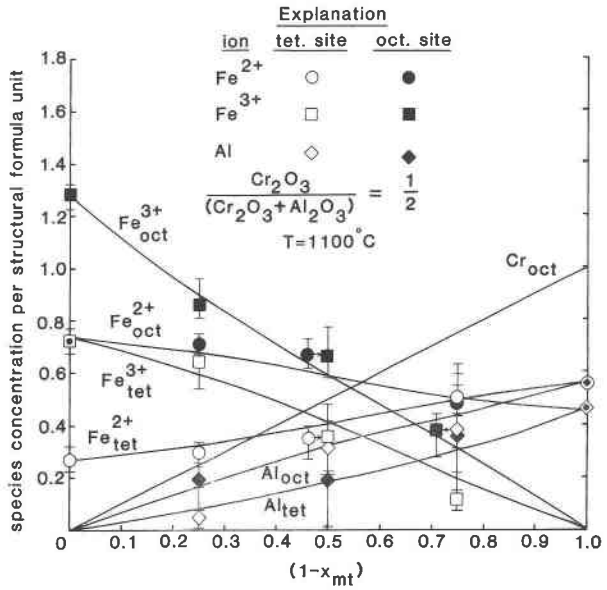

Fig. 10. Cation distributions along the pseudobinary system $(mt)_x(hc)_{1/2(1-x)}(ch)_{1/2(1-x)}$ at 1100 °C plotted as a function of (1 − mole fraction Fe_3O_4, i.e., $1 - X_{mt}$). Solid curves are model calculations.

through the relationships in Table 3. Uncertainties in the cation distributions were calculated by considering maximum uncertainties in the thermopower and conductivity measurements as outlined by Nell et al. (1989). Results for each system are presented in Figures 8A, 9, and 10 together with calculated distribution curves (see below).

Thermodynamic model

Our estimates of cation distributions may be combined with data on activity-composition relations and interphase partitioning to construct a thermodynamic model for $(Mg^{2+},Fe^{2+})(Fe^{3+},Al^{3+}Cr^{3+})_2O_4$ spinels that makes explicit provision for all order-disorder relations. We will commence with outlining the approach. The thermodynamic properties were formulated as an extension of our previous work on $(Mg^{2+},Fe^{2+})(Fe^{3+},Al^{3+})_2O_4$ solid solutions (Nell and Wood, 1989). There are ten independent fictive normal and inverse reference components in $(Mg^{2+},Fe^{2+})(Fe^{3+},Al^{3+}Cr^{3+})_2O_4$ solid solutions that were used to derive mixing properties (Table 4). The reference components are related through three independent compositional exchange vectors, $Fe^{2+}(Mg^{2+})_{-1}$, $Al^{3+}(Fe^{3+} + Cr^{3+})_{-1}$, and $Cr^{3+}(Al^{3+} + Fe^{3+})_{-1}$, and three compositional parameters are required to express the bulk chemical composition of any particular phase. These parameters are labeled r_1, r_2, and r_3 and are defined as follows:

$$r_1 = 1 - ({}^{[4]}X_{Mg} + 2{}^{[6]}X_{Mg})$$
$$r_2 = \tfrac{1}{2}({}^{[4]}X_{Al} + 2{}^{[6]}X_{Al})$$

and

$$r_3 = {}^{[6]}X_{Cr} \qquad (7)$$

where ${}^{[6]}X_{Cr}$ refers to the atomic fraction of Cr^{3+} on octahedral sites. There are also four intersite cation exchange reactions between the reference end-member components, three of which are independent. The three selected order parameters are labeled s_1, s_2, and s_3 and are defined as follows (s_3 was formulated as an absolute rather than a difference quantity in order to facilitate comparison between the series expansion model and our earlier O'Neill-Navrotsky formalism, Nell et al., 1989):

$$s_1 = {}^{[6]}X_{Al} - \tfrac{1}{2}{}^{[4]}X_{Al}$$
$$s_2 = {}^{[6]}X_{Fe^{3+}} - \tfrac{1}{2}{}^{[4]}X_{Fe^{3+}}$$

and

$$s_3 = 2{}^{[6]}X_{Mg}. \qquad (8)$$

Table 3. Compositional relations and constraints in Fe_3O_4-$FeCr_2O_4$, Fe_3O_4-$MgCr_2O_4$, and Fe_3O_4-$FeAl_2O_4$-$FeCr_2O_4$ solid solutions

System	$(Fe_3O_4)_x(FeCr_2O_4)_{1-x}$
Structural formula	$Fe_a^{2+}Fe_b^{3+}(Fe_d^{2+}Fe_e^{3+}Cr_n)_2O_4$
	$a + b = 1$
	$d + e + n = 2$
	$2(a + d) + 3(b + e + n) = 8$
	$b + e = 2x$
System	$(Fe_3O_4)_x(MgCr_2O_4)_{1-x}$
Structural formula	$Fe_a^{2+}Fe_b^{3+}Mg_c(Fe_d^{2+}Fe_e^{3+}Mg_fCr_n)_2O_4$
	$a + b + c = 1$
	$d + e + f + n = 2$
	$2(a + d + c + f) + 3(b + e + n) = 8$
	$a + b + d + e = 3x$
	$b + e = 2(a + d)$
System	$(Fe_3O_4)_x(FeAl_2O_4)_{y(1-x)}FeCr_2O_{4(1-y)(1-x)}$
Structural formula	$Fe_a^{2+}Fe_b^{3+}Al_c(Fe_d^{2+}Fe_e^{3+}Al_fCr_n)_2O_4$
	$a + b + c = 1$
	$d + e + f + n = 2$
	$2(a + d) + 3(b + c + e + f + n) = 8$
	$b + e = 2x$
	$(c + f)/(c + f + n) = y$

TABLE 4. Fictive end-members of normal and inverse spinel in Fe_3O_4-$FeAl_2O_4$-$MgFe_2O_4$-$MgAl_2O_4$-$FeCr_2O_4$-$MgCr_2O_4$ solid solutions

Component*	$Mg(Al)_2O_4$	$Al(MgAl)O_4$	$Fe^{2+}(Fe^{3+})_2O_4$	$Fe^{3+}(Fe^{2+}Fe^{3+})O_4$	$Fe^{2+}(Al)_2O_4$	$Al(Fe^{2+}Al)O_4$	$Mg(Fe^{3+})_2O_4$	$Fe^{3+}(MgFe^{3+})O_4$	$Fe(Cr)_2O_4$	$Mg(Cr)_2O_4$
Number	1	2	3	4	5	6	7	8	9	10
Parameter										
r_1	0	0	1	1	1	1	0	0	1	0
r_2	1	1	0	0	1	1	0	0	0	0
r_3	0	0	0	0	0	0	0	0	1	1
s_1	1	0	0	0	1	0	0	0	0	0
s_2	0	0	1	0	0	0	1	0	0	0
s_3	0	1	0	0	0	0	0	1	0	0

Note: Solid solutions expressed in terms of compositional and order parameters.
* Species in parentheses reside on octahedral sites.

Six parameters are thus required to characterize composition and order in $(Mg^{2+},Fe^{2+})(Fe^{3+},Al^{3+}Cr^{3+})_2O_4$ spinels. The coordinates of the reference components in the six parameter space are in Table 4, and cation fractions per structural formula unit are in Table 5. From the information in Table 5, the configurational entropy of a solid solution (S_{conf}) may be expressed as a function of order and compositional parameters through the equation

$$S_{conf} = -R \sum_a \sum_i n_a X_{i,a} \ln(X_{i,a}) \quad (9)$$

where n_a is the number of sites (a) per formula unit and $X_{i,a}$ is the mole fraction of component i on site a.

The vibrational part of the Gibbs free energy (G^*) is obtained from a second-degree Taylor series expansion in terms of compositional and order parameters (Thompson, 1969; Sack, 1982; Nell and Wood, 1989):

$$\begin{aligned} G^* = {} & g_0 + g_{r_1}r_1 + g_{r_2}r_2 + g_{r_3}r_3 + g_{s_1}s_1 + g_{s_2}s_2 + g_{s_3}s_3 \\ & + g_{r_1r_1}r_1^2 + g_{r_2r_2}r_2^2 + g_{r_3r_3}r_3^2 + g_{s_1s_1}s_1^2 + g_{s_2s_2}s_2^2 \\ & + g_{s_3s_3}s_3^2 + g_{r_1r_2}r_1r_2 + g_{r_1r_3}r_1r_3 + g_{r_1s_1}r_1s_1 \\ & + g_{r_1s_2}r_1s_2 + g_{r_1s_3}r_1s_3 + g_{r_2r_3}r_2r_3 + g_{r_2s_1}r_2s_1 \\ & + g_{r_2s_2}r_2s_2 + g_{r_2s_3}r_2s_3 + g_{r_3s_1}r_3s_1 + g_{r_3s_2}r_3s_2 \\ & + g_{r_3s_3}r_3s_3 + g_{s_1s_2}s_1s_2 + g_{s_1s_3}s_1s_3 + g_{s_2s_3}s_2s_3 \end{aligned} \quad (10)$$

where the g_n terms are series expansion coefficients. The Gibbs free energy (G) of a solid solution is then obtained from Equations 9 and 10 through the relation

$$G = G^* - TS_{conf}. \quad (11)$$

Nonideal mixing in the second-degree expansion can be identified with symmetric binary interaction parameters and reciprocal reaction terms (Thompson, 1969; Nell and Wood, 1989). In our previous paper, we derived a solution set for the 21 series expansion coefficients that do not involve the r_3 parameter. By considering the 17 possible binary solid solutions involving reference components $FeCr_2O_4$ and $MgCr_2O_4$ (Table 4), the coefficients involving the r_3 parameter were likewise determined. The complete set for the series expansion coefficients expressed in terms of on-site regular symmetric interaction parameters and reciprocal reaction energies is given in Appendix 1. The subscripts to the reciprocal reaction terms refer to the reference end-member components defined in Table 4, whereas the formulation of the reciprocal reaction terms and the interaction parameters were discussed in detail in our previous paper (Nell and Wood, 1989).

Equilibrium conditions

Equilibrium in $(Mg^{2+},Fe^{2+})(Fe^{3+},Al^{3+}Cr^{3+})_2O_4$ solid solutions is achieved when, at fixed temperature, pressure and composition, the following conditions are satisfied:

$$\left(\frac{\partial G}{\partial s_1}\right)_{T,P,r_1,r_2,r_3,s_2,s_3} = \left(\frac{\partial G}{\partial s_2}\right)_{T,P,r_1,r_2,r_3,s_1,s_3} = \left(\frac{\partial G}{\partial s_3}\right)_{T,P,r_1,r_2,r_3,s_1,s_3} = 0. \quad (12)$$

Substituting Equations 9 and 10 into 11 and differenti-

TABLE 5. Cation fractions per structural formula unit*

Ion	Tetrahedral site	Octahedral site	Sum
Mg	$1 - r_1 - s_3$	s_3	$1 - r_1$
Al	$r_2 - s_1$	$r_2 + s_1$	$2r_2$
Fe^{2+}	$r_1 + r_3 + s_1 + s_2 + s_3 - 1$	$1 - r_3 - s_1 - s_2 - s_3$	r_1
Fe^{3+}	$1 - s_2 - r_2 - r_3$	$1 + s_2 - r_2 - r_3$	$2 - 2r_2 - 2r_3$
Cr	0	$2r_3$	$2r_3$
Sum	1	2	3

* Given as a function of compositional parameters (r_1, r_2, and r_3) and order parameters (s_1, s_2, and s_3).

ating gives the equilibrium conditions in terms of expansion coefficients and cation site fractions:

$$\left(\frac{\partial G}{\partial s_1}\right)_{T,P,r_1,r_2,r_3,s_2,s_3} = g_{s_1} + 2g_{s_1s_1}s_1 + g_{r_1s_1}r_1 + g_{r_2s_1}r_2 + g_{r_3s_1}r_3 + g_{s_1s_2}s_2 + g_{s_1s_3}s_3 + RT\ln\frac{([4]Fe^{2+})([6]Al^{3+})}{([6]Fe^{2+})([4]Al^{3+})} = 0 \quad (13)$$

$$\left(\frac{\partial G}{\partial s_2}\right)_{T,P,r_1,r_2,r_3,s_1,s_3} = g_{s_2} + 2g_{s_2s_2}s_2 + g_{r_1s_2}r_1 + g_{r_2s_2}r_2 + g_{r_3s_2}r_3 + g_{s_1s_2}s_1 + g_{s_2s_3}s_3 + RT\ln\frac{([4]Fe^{2+})([6]Fe^{3+})}{([6]Fe^{2+})([4]Fe^{3+})} = 0 \quad (14)$$

and

$$\left(\frac{\partial G}{\partial s_3}\right)_{T,P,r_1,r_2,r_3,s_1,s_2} = g_{s_3} + 2g_{s_3s_3}s_3 + g_{r_1s_3}r_1 + g_{r_2s_3}r_2 + g_{r_3s_3}r_3 + g_{s_1s_3}s_1 + g_{s_2s_3}s_2 + RT\ln\frac{([4]Fe^{2+})([6]Mg^{2+})}{([6]Fe^{2+})([4]Mg^{2+})} = 0. \quad (15)$$

Equations 13–15 were used to calculate intersite cation distributions in $(Mg^{2+},Fe^{2+})(Fe^{3+},Al^{3+}Cr^{3+})_2O_4$ spinels after the following substitutions for the compositional parameters r_1 to r_3 were made:

$$r_1 = X_{Fe_3O_4} + X_{FeAl_2O_4} + X_{FeCr_2O_4}$$
$$r_2 = X_{FeAl_2O_4} + X_{MgAl_2O_4}$$

and

$$r_3 = X_{FeCr_2O_4} + X_{MgCr_2O_4}. \quad (16)$$

All but the $g_{r_3s_1}$, $g_{r_3s_2}$, and $g_{r_3s_3}$ parameters in Equations 13–15 were derived in our previous study (Nell and Wood, 1989). The new coefficients ($g_{r_3s_1}$, $g_{r_3s_2}$, and $g_{r_3s_3}$) describe the effects of Cr^{3+} substitution on intersite partitioning involving Fe^{2+}-Al^{3+}, Fe^{2+}-Fe^{3+}, and Fe^{2+}-Mg^{2+}, respectively. It follows therefore that, unless all these parameters are equal to zero, the substitution of Cr^{3+} must affect cation distributions despite the fact that it does not, itself, disorder.

Activity-composition relations

There are six compositional series expansion coefficients available to model activity-composition relations along the 15 binary solid solutions in the trigonal prism Fe_3O_4-$FeAl_2O_4$-$MgFe_2O_4$-$MgAl_2O_4$-$FeCr_2O_4$-$MgCr_2O_4$. The values of three of these coefficients were determined from our work in the quaternary $(Mg^{2+},Fe^{2+})(Fe^{3+},Al^{3+})_2O_4$ (Nell and Wood, 1989). Three additional coefficients ($g_{r_3r_3}$, $g_{r_1r_3}$, and $g_{r_2r_3}$) are required to describe activity-composition relations along the eight binary Cr-bearing solid solutions where the r_3 compositional exchange vector is operative.

Substituting Equations 9 and 10 into Equation 11 and differentiating with respect to r_1, r_2, and r_3 gives

$$\left(\frac{\partial G}{\partial r_1}\right)_{T,P,r_2,r_3,s_1,s_2,s_3} = g_{r_1} + 2g_{r_1r_1}r_1 + g_{r_1r_2}r_2 + g_{r_1r_3}r_3 + g_{r_1s_1}s_1 + g_{r_1s_2}s_2 + g_{r_1s_3}s_3 + RT\ln\frac{([4]Fe^{2+})}{([4]Mg^{2+})} \quad (17)$$

$$\left(\frac{\partial G}{\partial r_2}\right)_{T,P,r_1,r_3,s_1,s_2,s_3} = g_{r_2} + 2g_{r_2r_2}r_2 + g_{r_1r_2}r_1 + g_{r_2r_3}r_3 + g_{r_2s_1}s_1 + g_{r_2s_2}s_2 + g_{r_2s_3}s_3 + RT\ln\frac{([4]Al^{3+})([6]Al^{3+})}{([4]Fe^{3+})([6]Fe^{3+})} \quad (18)$$

and

$$\left(\frac{\partial G}{\partial r_3}\right)_{T,P,r_1,r_2,s_1,s_2,s_3} = g_{r_3} + 2g_{r_3r_3}r_3 + g_{r_1r_3}r_1 + g_{r_2r_3}r_2 + g_{r_3s_1}s_1 + g_{r_3s_2}s_2 + g_{r_3s_3}s_3 + RT\ln\frac{([4]Fe^{2+})([6]Cr^{3+})^2}{([4]Fe^{3+})([6]Fe^{3+})([6]Fe^{2+})}. \quad (19)$$

Chemical potentials of fictive reference components are obtained by partial differentiation of the free energy with respect to each of the order and compositional parameters:

$$\mu_{a,b,c,d,e,f} = G + (a - r_1)\left(\frac{\partial G}{\partial r_1}\right)_{T,P,r_2,r_3,s_1,s_2,s_3} + (b - r_2)\left(\frac{\partial G}{\partial r_2}\right)_{T,P,r_1,r_3,s_1,s_2,s_3} + (c - r_3)\left(\frac{\partial G}{\partial r_3}\right)_{T,P,r_1,r_2,s_1,s_2,s_3} + (d - s_1)\left(\frac{\partial G}{\partial s_1}\right)_{T,P,r_1,r_2,r_3,s_2,s_3} + (e - s_2)\left(\frac{\partial G}{\partial s_2}\right)_{T,P,r_1,r_2,r_3,s_1,s_3} + (f - s_3)\left(\frac{\partial G}{\partial s_3}\right)_{T,P,r_1,r_2,r_3,s_1,s_2} \quad (20)$$

where the coefficients a–f are coordinates of a phase in r_1-r_2-r_3-s_1-s_2-s_3 space. Chemical potentials of the reference end-member components obtained from Equation 20 are presented in Table 6. Reference components 1–8 are, of

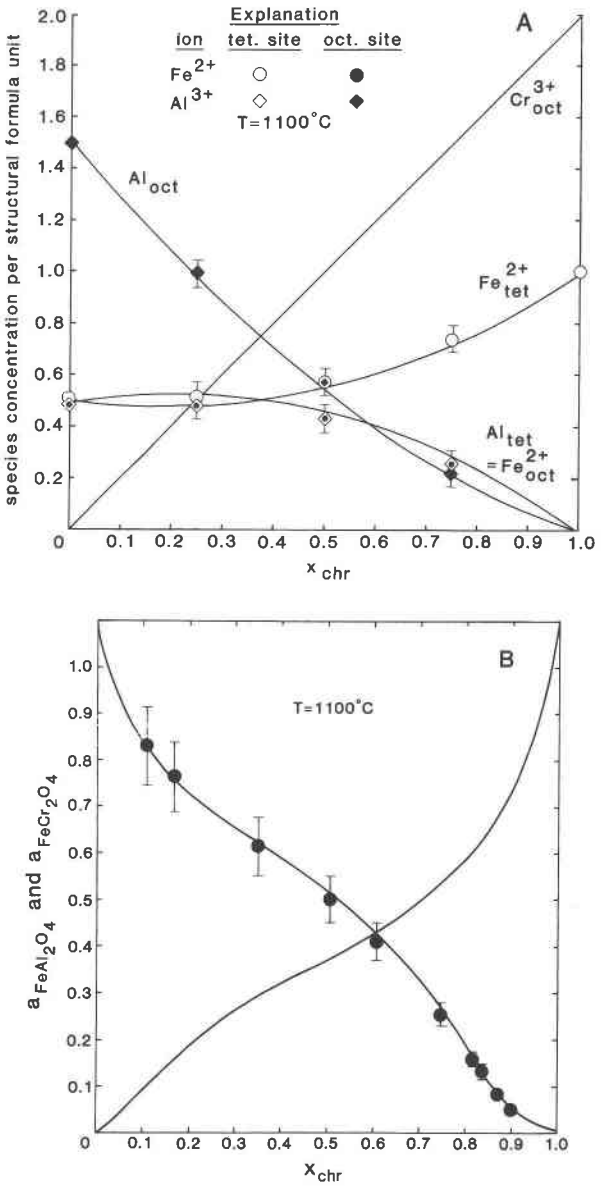

Fig. 11. (**A**) Cation distributions on the join $FeAl_2O_4$-$FeCr_2O_4$ at 1100 °C obtained from a Gibbs-Duhem integration of the partial molar magnetite entropies in Fe_3O_4-$FeAl_2O_4$-$FeCr_2O_4$ solid solutions. Results are plotted as a function of mole fraction $FeCr_2O_4$ (X_{chr}). Solid lines are model calculations. (**B**) Activity-composition relations in $FeAl_2O_4$-$FeCr_2O_4$ solid solutions at 1100 °C. Data are from Petric and Jacob (1982b) and solid lines are calculated from the model.

course, fictive and do not refer to the actual standard states of $MgAl_2O_4$, Fe_3O_4, $FeAl_2O_4$, and $MgFe_2O_4$ at the conditions of interest. Chemical potentials relative to real $MgAl_2O_4$, Fe_3O_4, $FeAl_2O_4$, and $MgFe_2O_4$ standard states at the conditions of interest are obtained through the substitution in Equation 20 of the values of the order and composition parameters *a–f*, which correspond to those end-members. The activities of $MgAl_2O_4$, Fe_3O_4, $FeAl_2O_4$, and $MgFe_2O_4$ relative to disordered pure end-member standard states at the temperature and pressure of interest as well as the activities of $FeCr_2O_4$ and $MgCr_2O_4$ relative to normal standard state end-members are in Table 7.

Constraint of model parameters

Values of the coefficients involving the r_3 parameter were derived as an extension of the parameters obtained in our earlier work (Nell and Wood, 1989). The $g_{r_3s_1}$ and $g_{r_3s_2}$ parameters were constrained from our cation distribution data for Fe_3O_4-$FeAl_2O_4$-$FeCr_2O_4$ and Fe_3O_4-$FeCr_2O_4$ solid solutions, respectively. Data for Fe_3O_4-$MgCr_2O_4$ solid solutions suggest that the $g_{r_3s_3}$ parameter is effectively equal to zero, indicating that the substitution of Cr^{3+} does not affect the partitioning of Fe^{2+} and Mg^{2+} between octahedral and tetrahedral sites (Eq. 15).

The $g_{r_3r_3}$ parameter was constrained from activity-composition relations in Fe_3O_4-$FeCr_2O_4$ solid solutions at 1227 °C (Katsura et al., 1975) and 1400 °C (Petric and Jacob, 1982a). The $g_{r_2r_3}$ coefficient was determined from Al^{3+}-Cr^{3+} partitioning experiments between clinopyroxene and $MgAl_2O_4$-$MgCr_2O_4$ solid solutions at 1100 °C (Webb and Wood, 1986), whereas $g_{r_1r_3}$ was estimated from experiments on the partitioning of Fe^{2+}-Mg^{2+} between olivine and $MgAl_2O_4$-$FeAl_2O_4$-$FeCr_2O_4$-$MgCr_2O_4$ solid solutions at 800 °C and 900 °C (Engi, 1983). The fitted values of the $g_{r_3r_3}$, $g_{r_3s_1}$, $g_{r_3s_2}$, $g_{r_3s_3}$, $g_{r_3r_3}$, $g_{r_1r_3}$, and $g_{r_2r_3}$ parameters were finally tested and refined by comparing observed and calculated cation distributions, activity-composition relations, and interphase partitioning coefficients in Fe_3O_4-$FeCr_2O_4$, Fe_3O_4-$MgCr_2O_4$, Fe_3O_4-$FeAl_2O_4$-$FeCr_2O_4$, $MgAl_2O_4$-$MgCr_2O_4$, and $FeAl_2O_4$-$FeCr_2O_4$ solid solutions. The standard state chemical potentials of the reference end-member components were set to zero and the values of the g_0, g_{r_1}, g_{r_2}, and g_{r_3} coefficients were subsequently constrained to be consistent with the values of the higher order expansion coefficients. These values are reported in Table 8 together with the values of the coefficients obtained in our earlier study (Nell and Wood, 1989). The estimated uncertainties in Table 8 reflect ranges over which the values may be varied while preserving a reasonable fit to the data. The coefficients are highly correlated (Nell and Wood, 1989) and the uncertainties are not intended to represent those correlations.

Application of the model to $FeCr_2O_4$- and $MgCr_2O_4$-bearing solid solutions

Cation distributions and activity-composition relations in Fe_3O_4-$FeCr_2O_4$, Fe_3O_4-$MgCr_2O_4$, Fe_3O_4-$FeAl_2O_4$-$FeCr_2O_4$, and $MgAl_2O_4$-$MgCr_2O_4$ solid solutions were calculated from the values of the expansion coefficients in Table 8. Equations 13–15 were used to calculate cation distributions for a given temperature. A Newton-Raphson method (e.g., Gerald and Wheatley, 1984, p. 133–159) was used to solve the nonlinear equations resulting in the solid lines in Figures 8A, 9, 10, and 11A. In all four systems, the data were used to constrain model pa-

TABLE 6. Chemical potentials of reference end-member components

$$
\begin{aligned}
\mu_{Al(MgAl)O_4} &= g_0 + g_{r_2} + g_{s_3} - g_{r_1r_1}r_1^2 - g_{r_2r_2}r_2^2 - g_{s_1s_1}s_1^2 - g_{s_2s_2}s_2^2 - g_{s_3s_3}s_3^2 \\
&\quad - g_{r_1s_1}r_1s_1 - g_{r_1s_2}r_1s_2 - g_{s_1s_2}s_1s_2 + (2g_{r_2r_2} + g_{r_2s_3})r_2 + (g_{r_1r_2} + g_{r_1s_3})r_1 \\
&\quad + (g_{r_2s_1} + g_{s_1s_3})s_1 + (g_{r_2s_2} + g_{s_2s_3})s_2 + (2g_{s_3s_3} + g_{r_2s_3})s_3 - g_{r_1r_2}r_1r_2 \\
&\quad - g_{r_2s_2}r_2s_1 - g_{r_2s_2}r_2s_2 - g_{r_1s_3}r_1s_3 - g_{r_2s_3}r_2s_3 - g_{s_1s_3}s_1s_3 - g_{s_2s_3}s_2s_3 \\
&\quad - g_{r_3r_3}r_3^2 - g_{r_1r_3}r_1r_3 + (g_{r_2r_3} + g_{r_3s_3})r_3 - g_{r_2r_3}r_2r_3 \\
&\quad - g_{r_3s_1}r_3s_1 - g_{r_3s_2}r_3s_2 - g_{r_3s_3}r_3s_3 \\
&\quad + RT[\ln([4]Al)([6]Al)([6]Mg) - 2\ln 2] \\
\mu_{Mg(AlAl)O_4} &= g_0 + g_{r_2} + g_{s_1} - g_{r_1r_1}r_1^2 - g_{r_2r_2}r_2^2 - g_{s_1s_1}s_1^2 - g_{s_2s_2}s_2^2 - g_{s_3s_3}s_3^2 \\
&\quad - g_{r_1s_2}r_1s_2 - g_{r_1s_3}r_1s_3 - g_{s_2s_3}s_2s_3 + (2g_{r_2r_2} + g_{r_2s_1})r_2 + (g_{r_1r_2} + g_{r_1s_1})r_1 \\
&\quad + (g_{r_2s_1} + 2g_{s_1s_1})s_1 + (g_{r_2s_2} + g_{s_1s_2})s_2 + (g_{s_1s_3} + g_{r_2s_3})s_3 - g_{r_1r_2}r_1r_2 \\
&\quad - g_{r_2s_1}r_2s_1 - g_{r_2s_2}r_2s_2 - g_{r_1s_1}r_1s_1 - g_{r_2s_3}r_2s_3 - g_{s_1s_3}s_1s_3 - g_{s_1s_2}s_1s_2 \\
&\quad - g_{r_3r_3}r_3^2 - g_{r_1r_3}r_1r_3 - g_{r_2r_3}r_2r_3 + (g_{r_2r_3} + g_{r_3s_1})r_3 \\
&\quad - g_{r_3s_1}r_3s_1 - g_{r_3s_2}r_3s_2 - g_{r_3s_3}r_3s_3 \\
&\quad + RT[2\ln([6]Al) + \ln([4]Mg) - 2\ln 2] \\
\mu_{Fe^{3+}(Fe^{2+}Fe^{3+})O_4} &= g_0 + g_{r_1} - g_{r_1r_1}r_1^2 - g_{r_2r_2}r_2^2 - g_{s_1s_1}s_1^2 - g_{s_2s_2}s_2^2 - g_{s_3s_3}s_3^2 \\
&\quad - 2g_{r_1r_1}r_1 + g_{r_1r_2}r_2 + g_{r_1s_1}s_1 + g_{r_1s_2}s_2 + g_{r_1s_3}s_3 - g_{r_1r_2}r_1r_2 - g_{r_1s_1}r_1s_1 \\
&\quad - g_{r_2s_1}r_2s_1 - g_{r_1s_2}r_1s_2 - g_{r_2s_2}r_2s_2 - g_{s_1s_2}s_1s_2 - g_{s_2s_3}s_2s_3 \\
&\quad - g_{r_1s_3}r_1s_3 - g_{r_2s_3}r_2s_3 - g_{s_1s_3}s_1s_3 - g_{r_3r_3}r_3^2 + g_{r_1r_3}r_3(1 - r_1) \\
&\quad - g_{r_2r_3}r_2r_3 - g_{r_3s_1}r_3s_1 - g_{r_3s_2}r_3s_2 - g_{r_3s_3}r_3s_3 \\
&\quad + RT[\ln([6]Fe^{3+})([4]Fe^{3+})([6]Fe^{2+}) - 2\ln 2] \\
\mu_{Fe^{2+}(Fe^{3+}Fe^{3+})O_4} &= g_0 + g_{r_1} + g_{s_2} - g_{r_1r_1}r_1^2 - g_{r_2r_2}r_2^2 - g_{s_1s_1}s_1^2 - g_{s_2s_2}s_2^2 - g_{s_3s_3}s_3^2 \\
&\quad + (2g_{r_1r_1} + g_{r_1s_2})r_1 + (g_{r_1r_2} + g_{r_2s_2})r_2 + (g_{r_1s_1} + g_{s_1s_2})s_1 + (g_{r_1s_2} + 2g_{s_2s_2})s_2 \\
&\quad + (g_{r_1s_3} + g_{s_2s_3})s_3 - g_{r_1r_2}r_1r_2 - g_{r_1s_1}r_1s_1 - g_{r_2s_1}r_2s_1 - g_{r_1s_2}r_1s_2 - g_{r_2s_2}r_2s_2 \\
&\quad - g_{s_1s_2}s_1s_2 - g_{s_2s_3}s_2s_3 - g_{r_1s_3}r_1s_3 - g_{r_2s_3}r_2s_3 - g_{s_1s_3}s_1s_3 - g_{r_3r_3}r_3^2 \\
&\quad + (g_{r_1r_3} + g_{r_3s_2})r_3 - g_{r_1r_3}r_1r_3 - g_{r_2r_3}r_2r_3 - g_{r_3s_1}r_3s_1 - g_{r_3s_2}r_3s_2 - g_{r_3s_3}r_3s_3 \\
&\quad + RT[2\ln([6]Fe^{3+}) + \ln([4]Fe^{2+}) - 2\ln 2] \\
\mu_{Al(Fe^{2+}Al)O_4} &= g_0 + g_{r_1} + g_{r_2} - g_{r_1r_1}r_1^2 - g_{r_2r_2}r_2^2 - g_{s_1s_1}s_1^2 - g_{s_2s_2}s_2^2 - g_{s_3s_3}s_3^2 \\
&\quad + (2g_{r_1r_1} + g_{r_1r_2})r_1 + (2g_{r_2r_2} + g_{r_1r_2})r_2 + (g_{r_1s_1} + g_{r_2s_1})s_1 + (g_{r_1s_2} + g_{r_2s_2})s_2 \\
&\quad + (g_{r_1s_3} + g_{r_2s_3} + g_{s_1s_3})s_3 - g_{r_1r_2}r_1r_2 - g_{r_1s_1}r_1s_1 - g_{r_1s_2}r_1s_2 - g_{r_1s_3}r_1s_3 \\
&\quad - g_{r_2s_1}r_2s_1 - g_{r_2s_2}r_2s_2 - g_{r_2s_3}r_2s_3 - g_{s_1s_2}s_1s_2 - g_{s_1s_3}s_1s_3 - g_{s_2s_3}s_2s_3 \\
&\quad - g_{r_3r_3}r_3^2 - (g_{r_1r_3} + g_{r_2r_3})r_3 - g_{r_1r_3}r_1r_3 - g_{r_2r_3}r_2r_3 \\
&\quad - g_{r_3s_1}r_3s_1 - g_{r_3s_2}r_3s_2 - g_{r_3s_3}r_3s_3 \\
&\quad + RT[\ln([6]Fe^{2+})([6]Al)([4]Al) - 2\ln 2] \\
\mu_{Fe^{2+}(AlAl)O_4} &= g_0 + g_{r_1} + g_{r_2} + g_{s_1} - g_{r_1r_1}r_1^2 - g_{r_2r_2}r_2^2 - g_{s_1s_1}s_1^2 - g_{s_2s_2}s_2^2 - g_{s_3s_3}s_3^2 \\
&\quad + (2g_{r_1r_1} + g_{r_1r_2} + g_{r_1s_1})r_1 + (2g_{r_2r_2} + g_{r_1r_2} + g_{r_2s_1})r_2 \\
&\quad + (2g_{s_1s_1} + g_{r_1s_1} + g_{r_2s_1})s_1 + (g_{r_1s_2} + g_{r_2s_2} + g_{s_1s_2})s_2 \\
&\quad + (g_{r_1s_3} + g_{r_2s_3} + g_{s_1s_3})s_3 - g_{r_1r_2}r_1r_2 - g_{r_1s_1}r_1s_1 - g_{r_1s_2}r_1s_2 - g_{r_1s_3}r_1s_3 \\
&\quad - g_{r_2s_1}r_2s_1 - g_{r_2s_2}r_2s_2 - g_{r_2s_3}r_2s_3 - g_{s_1s_2}s_1s_2 - g_{s_1s_3}s_1s_3 - g_{s_2s_3}s_2s_3 \\
&\quad - g_{r_3r_3}r_3^2 - (g_{r_1r_3} + g_{r_2r_3} + g_{r_3s_1})r_3 - g_{r_1r_3}r_1r_3 - g_{r_2r_3}r_2r_3 \\
&\quad - g_{r_3s_1}r_3s_1 - g_{r_3s_2}r_3s_2 - g_{r_3s_3}r_3s_3 \\
&\quad + RT[2\ln([6]Al) + \ln([4]Fe^{2+}) - 2\ln 2] \\
\mu_{Fe^{3+}(Fe^{3+}Mg)O_4} &= g_0 + g_{s_3} - g_{r_1r_1}r_1^2 - g_{r_2r_2}r_2^2 - g_{s_1s_1}s_1^2 - g_{s_2s_2}s_2^2 - g_{s_3s_3}s_3^2 \\
&\quad + g_{r_1s_3}r_1 + g_{r_2s_3}r_2 + g_{s_1s_3}s_1 + g_{s_2s_3}s_2 + 2g_{s_3s_3}s_3 \\
&\quad - g_{r_1r_2}r_1r_2 - g_{r_1s_1}r_1s_1 - g_{r_1s_2}r_1s_2 - g_{r_1s_3}r_1s_3 - g_{r_2s_1}r_2s_1 \\
&\quad - g_{r_2s_2}r_2s_2 - g_{r_2s_3}r_2s_3 - g_{s_1s_2}s_1s_2 - g_{s_1s_3}s_1s_3 - g_{s_2s_3}s_2s_3 \\
&\quad - g_{r_3r_3}r_3^2 - g_{r_1r_3}r_1r_3 - g_{r_2r_3}r_2r_3 - g_{r_3s_1}r_3s_1 \\
&\quad - g_{r_3s_2}r_3s_2 - g_{r_3s_3}r_3(s_3 - 1) \\
&\quad + RT[\ln([4]Fe^{3+})([6]Fe^{3+})([6]Mg) - 2\ln 2] \\
\mu_{Mg(Fe^{3+}Fe^{3+})O_4} &= g_0 + g_{s_2} - g_{r_1r_1}r_1^2 - g_{r_2r_2}r_2^2 - g_{s_1s_1}s_1^2 - g_{s_2s_2}s_2^2 - g_{s_3s_3}s_3^2 \\
&\quad + g_{r_1s_2}r_1 + g_{r_2s_2}r_2 + g_{s_1s_2}s_1 + 2g_{s_2s_2}s_2 + g_{s_2s_3}s_3 \\
&\quad - g_{r_1r_2}r_1r_2 - g_{r_1s_1}r_1s_1 - g_{r_1s_2}r_1s_2 - g_{r_1s_3}r_1s_3 - g_{r_2s_1}r_2s_1 \\
&\quad - g_{r_2s_2}r_2s_2 - g_{r_2s_3}r_2s_3 - g_{s_1s_2}s_1s_2 - g_{s_1s_3}s_1s_3 - g_{s_2s_3}s_2s_3 \\
&\quad - g_{r_3r_3}r_3^2 - g_{r_1r_3}r_1r_3 - g_{r_2r_3}r_2r_3 - g_{r_3s_1}r_3s_1 \\
&\quad - g_{r_3s_2}r_3(s_2 - 1) - g_{r_3s_3}r_3s_3 \\
&\quad + RT[2\ln([6]Fe^{3+}) + \ln([4]Mg) - 2\ln 2] \\
\mu_{FeCr_2O_4} &= g_0 + g_{r_1} + g_{r_3} - g_{r_1r_1}r_1^2 - g_{r_2r_2}r_2^2 - g_{r_3r_3}r_3^2 - g_{s_1s_1}s_1^2 - g_{s_2s_2}s_2^2 \\
&\quad - g_{s_3s_3}s_3^2 + (2g_{r_1r_1} + g_{r_1r_3})r_1 + (g_{r_1r_2} + g_{r_2r_3})r_2 + (2g_{r_3r_3} + g_{r_1r_3})r_3 \\
&\quad + (g_{r_1s_1} + g_{r_3s_1})s_1 + (g_{r_1s_2} + g_{r_3s_2})s_2 + (g_{r_1s_3} + g_{r_3s_3})s_3 - g_{r_1r_2}r_1r_2 \\
&\quad - g_{r_1r_3}r_1r_3 - g_{r_1s_1}r_1s_1 - g_{r_1s_2}r_1s_2 - g_{r_1s_3}r_1s_3 - g_{r_2r_3}r_2r_3 \\
&\quad - g_{r_2s_1}r_2s_1 - g_{r_2s_2}r_2s_2 - g_{r_2s_3}r_2s_3 - g_{r_3s_1}r_3s_1 - g_{r_3s_2}r_3s_2 \\
&\quad - g_{r_3s_3}r_3s_3 - g_{s_1s_2}s_1s_2 - g_{s_1s_3}s_1s_3 - g_{s_2s_3}s_2s_3 \\
&\quad + RT[2\ln([6]Cr) + \ln([4]Fe^{2+}) - 2\ln 2] \\
\mu_{MgCr_2O_4} &= g_0 + g_{r_3} - g_{r_1r_1}r_1^2 - g_{r_2r_2}r_2^2 - g_{r_3r_3}r_3^2 - g_{s_1s_1}s_1^2 - g_{s_2s_2}s_2^2 \\
&\quad - g_{s_3s_3}s_3^2 + 2g_{r_3r_3}r_3 - g_{r_1r_2}r_1r_2 + g_{r_1r_3}r_1(1 - r_3) - g_{r_1s_1}r_1s_1 \\
&\quad - g_{r_1s_2}r_1s_2 - g_{r_1s_3}r_1s_3 + g_{r_2r_3}r_2(1 - r_3) - g_{r_2s_1}r_2s_1 - g_{r_2s_2}r_2s_2 \\
&\quad - g_{r_2s_3}r_2s_3 + g_{r_3s_1}s_1(1 - r_3) + g_{r_3s_2}s_2(1 - r_3) + g_{r_3s_3}s_3(1 - r_3) \\
&\quad - g_{s_1s_2}s_1s_2 - g_{s_1s_3}s_1s_3 - g_{s_2s_3}s_2s_3 \\
&\quad + RT[2\ln([6]Cr) + \ln([4]Mg) - 2\ln 2]
\end{aligned}
$$

rameters, and the calculated lines are thus fitted. Fe_3O_4, $FeAl_2O_4$, $MgFe_2O_4$, $MgAl_2O_4$, $FeCr_2O_4$, and $MgCr_2O_4$ activities were calculated from the equations in Tables 6 and 7 and are presented as solid lines in activity-composition diagrams (Figs. 8B and 11B) and interphase partition plots (Figs. 12, 13A, and 13B). The data in Figures 8B and 13A were used to derive values of the model coefficients and the calculated lines in these figures are

TABLE 7. Activities of spinel, magnetite, hercynite, magnesioferrite, chromite and picrochromite relative end-member standard states at the temperature and pressures of interest

$$
\begin{aligned}
RT\ln a_{MgAl_2O_4} = & -g_{r_1r_1}r_1^2 - g_{r_2r_2}(r_2-1)^2 - g_{s_1s_1}[s_1(s_1-2+2s_3) - s_1^0(s_1^0-2+2s_3^0)] \\
& - g_{s_2s_2}s_2^2 - g_{s_3s_3}(s_3-s_3^0)^2 - g_{r_1r_2}r_1(r_2-1) - g_{r_1s_1}r_1(s_1+s_3^0-1) \\
& - g_{r_1s_2}r_1s_2 - g_{r_1s_3}r_1(s_3-s_3^0) - g_{r_2s_1}(r_2-1)(s_1+s_3^0-1) - g_{r_2s_2}s_2(r_2-1) \\
& - g_{r_2s_3}(r_2-1)(s_3-s_3^0) - g_{s_1s_2}s_2(s_1+s_3^0-1) - g_{s_1s_3}(s_3-s_3^0)(s_1+s_3^0+1) \\
& - g_{s_2s_3}s_2(s_3-s_3^0) - g_{r_3r_3}r_3^2 - g_{r_1r_3}r_1r_3 + g_{r_2r_3}r_3(1-r_2) \\
& - g_{r_3s_1}r_3(s_1+s_3^0-1) - g_{r_3s_2}r_3s_2 - g_{r_3s_3}r_3(s_3-s_3^0) \\
& + RT\left\{(1-s_3^0)\left[2\ln\frac{([6]Al)^{ss}}{([6]Al)^{sp}} + \ln\frac{([4]Mg)^{ss}}{([4]Mg)^{sp}}\right]\right\} \\
& + RT\left\{s_3^0\ln\frac{[([4]Al)([6]Al)([6]Mg)]^{ss}}{[([4]Al)([6]Al)([6]Mg)]^{sp}}\right\}
\end{aligned}
$$

$$
\begin{aligned}
RT\ln a_{Fe_3O_4} = & -g_{r_1r_1}(r_1-1)^2 - g_{r_2r_2}r_2^2 - g_{s_1s_1}s_1^2 - g_{s_2s_2}(s_2-s_2^0)^2 - g_{r_1r_2}r_2(r_1-1) \\
& - g_{s_3s_3}s_3^2 - g_{r_1s_1}s_1(r_1-1) - g_{r_1s_2}(r_1-1)(s_2-s_2^0) - g_{r_1s_3}s_3(r_1-1) \\
& - g_{r_2s_1}r_2s_1 - g_{r_2s_2}r_2(s_2-s_2^0) - g_{r_2s_3}r_2s_3 - g_{s_1s_2}s_1(s_2-s_2^0) \\
& - g_{s_1s_3}s_1s_3 - g_{s_2s_3}s_3(s_2-s_2^0) - g_{r_3r_3}r_3^2 - g_{r_2r_3}r_2r_3 - g_{r_3s_1}r_3s_1 \\
& - g_{r_3s_2}r_3s_3 + g_{r_1r_3}r_3(1-r_1) - g_{r_3s_2}r_3(s_2-s_2^0) \\
& + RT\left\{s_2^0\left[2\ln\frac{([6]Fe^{3+})^{ss}}{([6]Fe^{3+})^{mt}} + \ln\frac{([4]Fe^{2+})^{ss}}{([4]Fe^{2+})^{mt}}\right]\right\} \\
& + RT\left\{(1-s_2^0)\ln\frac{[([6]Fe^{3+})([4]Fe^{3+})([6]Fe^{2+})]^{ss}}{[([6]Fe^{3+})([4]Fe^{3+})([6]Fe^{2+})]^{mt}}\right\}
\end{aligned}
$$

$$
\begin{aligned}
RT\ln a_{FeAl_2O_4} = & -g_{r_1r_1}(r_1-1)^2 - g_{r_2r_2}(r_2-1)^2 - g_{s_1s_1}(s_1-s_1^0)^2 - g_{s_2s_2}s_2^2 \\
& - g_{s_3s_3}s_3^2 - g_{r_1r_2}(r_1r_2 - r_1 - r_2 + 1) - g_{r_1s_1}(r_1-1)(s_1-s_1^0) \\
& - g_{r_1s_2}s_2(r_1-1) - g_{r_1s_3}s_3(r_1-1) - g_{r_2s_1}(r_2-1)(s_1-s_1^0) \\
& - g_{r_2s_2}s_2(r_2-1) - g_{r_2s_3}s_3(r_2-1) - g_{s_1s_2}s_2(s_1-s_1^0) \\
& - g_{s_1s_3}s_3(s_1-s_1^0) - g_{s_2s_3}s_2s_3 - g_{r_3r_3}r_3^2 + g_{r_1r_3}r_3(1-r_1) \\
& + g_{r_2r_3}r_3(1-r_2) - g_{r_3s_1}r_3(s_1-s_1^0) - g_{r_3s_2}r_3s_2 - g_{r_3s_3}r_3s_3 \\
& + RT\left\{s_1^0\left[2\ln\frac{([6]Al)^{ss}}{([6]Al)^{hc}} + \ln\frac{([4]Fe^{2+})^{ss}}{([4]Fe^{2+})^{hc}}\right]\right\} \\
& + RT\left\{(1-s_1^0)\ln\frac{[([6]Al)([4]Al)([6]Fe^{2+})]^{ss}}{[([6]Al)([4]Al)([6]Fe^{2+})]^{hc}}\right\}
\end{aligned}
$$

$$
\begin{aligned}
RT\ln a_{MgFe_2O_4} = & -g_{r_1r_1}r_1^2 - g_{r_2r_2}r_2^2 - g_{s_1s_1}s_1^2 - g_{r_1r_2}r_1r_2 \\
& - g_{s_2s_2}[s_2(s_2-2+2s_3^0) - s_2^0(s_2^0-2+2s_3^0)] - g_{s_3s_3}(s_3-s_3^0)^2 \\
& - g_{r_1s_1}r_1s_1 - g_{r_1s_2}r_1(s_2+s_3^0-1) - g_{r_1s_3}r_1(s_3-s_3^0) - g_{r_2s_1}r_2s_1 \\
& - g_{r_2s_2}r_2(s_2+s_3^0-1) - g_{r_2s_3}r_2(s_3-s_3^0) - g_{s_1s_2}s_1(s_2+s_3^0-1) \\
& - g_{s_1s_3}s_1(s_3-s_3^0) - g_{s_2s_3}(s_3-s_3^0)(s_2+s_3^0-1) - g_{r_3r_3}r_3^2 \\
& - g_{r_1r_3}r_1r_3 - g_{r_2r_3}r_2r_3 - g_{r_3s_1}r_3s_1 - g_{r_3s_2}r_3(s_2+s_3^0-1) \\
& - g_{r_3s_3}r_3(s_3-s_3^0) \\
& + RT\left\{(1-s_3^0)\left[2\ln\frac{([6]Fe^{3+})^{ss}}{([6]Fe^{3+})^{mf}} + \ln\frac{([4]Mg)^{ss}}{([4]Mg)^{mf}}\right]\right\} \\
& + RT\left\{s_3^0\ln\frac{[([4]Fe^{3+})([6]Fe^{3+})([6]Mg)]^{ss}}{[([4]Fe^{3+})([6]Fe^{3+})([6]Mg)]^{mf}}\right\}
\end{aligned}
$$

$$
\begin{aligned}
RT\ln a_{FeCr_2O_4} = & -g_{r_1r_1}r_1^2 - g_{r_2r_2}r_2^2 - g_{r_3r_3}r_3^2 - g_{s_1s_1}s_1^2 - g_{s_2s_2}s_2^2 \\
& - g_{s_3s_3}s_3^2 + g_{r_1r_1}(2r_1-1) + g_{r_3r_3}(2r_3-1) + g_{r_1r_2}r_2(1-r_1) \\
& + g_{r_1r_3}(r_1+r_3-r_1r_3-1) + g_{r_1s_1}s_1(1-r_1) \\
& + g_{r_1s_2}s_2(1-r_1) + g_{r_1s_3}s_3(1-r_1) + g_{r_2r_3}r_2(1-r_3) - g_{r_2s_1}r_2s_1 \\
& - g_{r_2s_2}r_2s_2 - g_{r_2s_3}r_2s_3 + g_{r_3s_1}s_1(1-r_3) + g_{r_3s_2}s_2(1-r_3) \\
& + g_{r_3s_3}s_3(1-r_3) - g_{s_1s_2}s_1s_2 - g_{s_1s_3}s_1s_3 - g_{s_2s_3}s_2s_3 \\
& + RT\{2\ln([6]Cr)^{ss} + \ln([4]Fe^{2+})^{ss} - 2\ln 2\}
\end{aligned}
$$

$$
\begin{aligned}
RT\ln a_{MgCr_2O_4} = & -g_{r_1r_1}r_1^2 - g_{r_2r_2}r_2^2 - g_{r_3r_3}r_3^2 - g_{s_1s_1}s_1^2 - g_{s_2s_2}s_2^2 \\
& - g_{s_3s_3}s_3^2 + g_{r_3r_3}(2r_3-1) - g_{r_1r_2}r_1r_2 + g_{r_1r_3}r_1(1-r_3) - g_{r_1s_1}r_1s_1 \\
& - g_{r_1s_2}r_1s_2 - g_{r_1s_3}r_1s_3 + g_{r_2r_3}r_2(1-r_3) - g_{r_2s_1}r_2s_1 - g_{r_2s_2}r_2s_2 \\
& - g_{r_2s_3}r_2s_3 + g_{r_3s_1}s_1(1-r_3) + g_{r_3s_2}s_2(1-r_3) + g_{r_3s_3}s_3(1-r_3) \\
& - g_{s_1s_2}s_1s_2 - g_{s_1s_3}s_1s_3 - g_{s_2s_3}s_2s_3 \\
& + RT\{2\ln([6]Cr)^{ss} + \ln([4]Mg)^{ss} - 2\ln 2\}
\end{aligned}
$$

Note: The superscripts ss, sp, mt, hc, and mf refer, respectively, to solid solutions, pure spinel, pure magnetite, pure hercynite, and pure magnesioferrite, wherease the superscript 0 on the order parameters s_1, s_2, and s_3 indicates values in pure disordered end-member spinels.

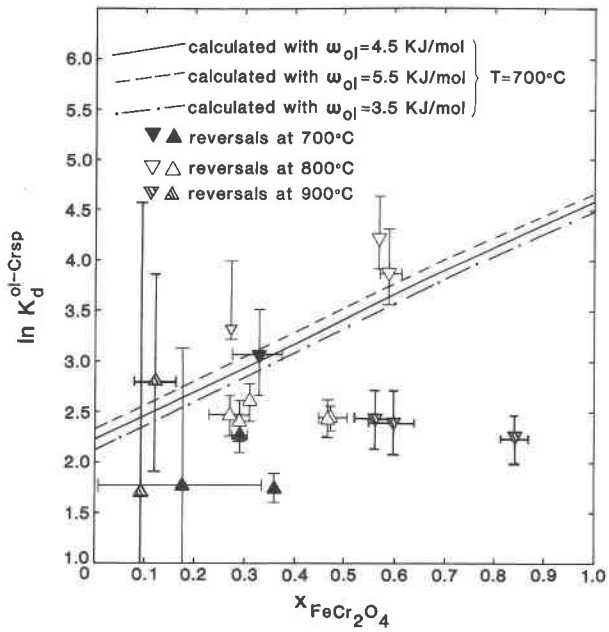

Fig. 12. Predicted values of ln $K_d^{ol-Crsp}$ [$K_d = (X^{Crsp}_{FeCr_2O_4})\cdot(X^{ol}_{MgSi_{0.5}O_2})/(X^{Crsp}_{MgCr_2O_4})\cdot(X^{ol}_{FeSi_{0.5}O_2})$] compared to the data of Engi (1983) at 700 °C, 800 °C, and 900 °C. Calculations were performed at 700 °C and take account of the nonideality (W_{ol} on a 1 atom basis) in olivine. Directions of approach to equilibrium in the experimental measurements are indicated by arrows on the error bars.

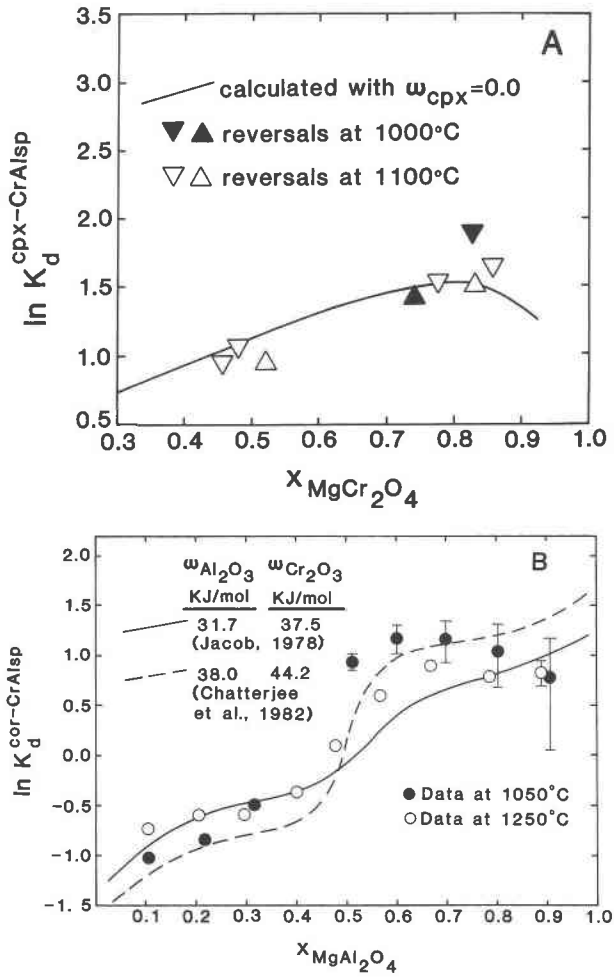

Fig. 13. (A) Calculated values of ln $K_d^{cpx-CrAlsp}$ [$K_d = (X^{CrAlsp}_{MgCr_2O_4})\cdot(X^{cpx}_{NaAlSi_2O_6})/(X^{CrAlsp}_{MgAl_2O_4})\cdot(X^{cpx}_{NaCrSi_2O_6})$] at 1100 °C compared to the data of Webb and Wood (1986) at 1000 °C and 1100 °C. Cr^{3+}-Al^{3+} mixing in clinopyroxene is assumed to be ideal. (B) Predicted values of ln $K_d^{cor-CrAlsp}$ [$K_d = (X^{CrAlsp}_{MgCr_2O_4})\cdot(X^{cor}_{Al_2O_3})/(X^{CrAlsp}_{MgAl_2O_4})\cdot(X^{cor}_{Cr_2O_3})$] at 1050 °C compared to the data of Oka et al. (1984) at 1050 °C and 1250 °C. Nonideality in Al_2O_3-Cr_2O_3 solid solutions is modeled with asymmetric interaction parameters.

TABLE 8. Internally consistent values of the Taylor series expansion coefficients

Coefficient	Value (kJ/mol)
g_0	2.9 ± 5.5
g_{r_1}	7.1 ± 4.5
g_{r_2}	33.5 ± 19.8
g_{r_3}	35.5 ± 2.5
g_{s_1}	14.7 ± 0.5
g_{s_2}	44.5 ± 4.5
g_{s_3}	34.0 ± 2.5
$g_{r_1r_1}$	−10.0 ± 1.0
$g_{r_2r_2}$	−38.0 ± 2.0
$g_{r_3r_3}$	−35.0 ± 2.0
$g_{s_1s_1}$	−25.7 ± 1.5
$g_{s_2s_2}$	−26.6 ± 1.3
$g_{s_3s_3}$	−15.0 ± 3.0
$g_{r_1r_2}$	10.0 ± 3.0
$g_{r_1r_3}$	−0.5 ± 0.2
$g_{r_1s_1}$	−7.1 ± 0.5
$g_{r_1s_2}$	−25.0 ± 3.5
$g_{r_1s_3}$	−15.0 ± 2.0
$g_{r_2r_3}$	−25.0 ± 2.0
$g_{r_2s_1}$	5.5 ± 3.0
$g_{r_2s_2}$	−16.6 ± 4.0
$g_{r_2s_3}$	−11.9 ± 2.0
$g_{r_3s_1}$	−24.8 ± 1.5
$g_{r_3s_2}$	−38.0 ± 1.0
$g_{r_3s_3}$	0.0 ± 1.0
$g_{s_1s_2}$	−16.0 ± 12.0
$g_{s_1s_3}$	−15.0 ± 3.0
$g_{s_2s_3}$	−24.6 ± 2.0

therefore fitted. The solid lines in Figures 11B, 12, and 13B are predicted because the data shown were not used to constrain model parameters.

$FeCr_2O_4$-$MgCr_2O_4$-$MgAl_2O_4$-$FeAl_2O_4$ solid solutions

Engi (1983) performed experiments on the exchange of Fe^{2+}-Mg^{2+} between olivine and $FeCr_2O_4$-$MgCr_2O_4$ solid solutions and between olivine and (Fe^{2+},Mg^{2+})-$(Al^{3+},Cr^{3+})_2O_4$ solid solutions with approximate compositions at the intersection of the $FeCr_2O_4$-$MgAl_2O_4$ and $MgCr_2O_4$-$FeAl_2O_4$ tie lines at temperatures ranging between 650 °C and 900 °C and pressures between 300 and 1000 bars. There is no cation disordering in the system $FeCr_2O_4$-$MgCr_2O_4$ and the only adjustable parameter in

the modeling of activity-composition relations along this binary is the $g_{r_1r_1}$ coefficient which has been constrained by the mixing properties of Fe_3O_4-$MgFe_2O_4$ and $MgAl_2O_4$-$FeAl_2O_4$ solid solutions (Nell and Wood, 1989). Fe^{2+}-Mg^{2+} partitioning between olivine (ol) and $FeCr_2O_4$-$MgCr_2O_4$ solid solution (Crsp) is given by

$$\ln K_d^{ol-Crsp} = \ln \frac{(X^{Crsp}_{FeCr_2O_4})(X^{ol}_{MgSi_{0.5}O_2})}{(X^{Crsp}_{MgCr_2O_4})(X^{ol}_{FeSi_{0.5}O_2})}$$

$$= \ln K_a^{ol-Crsp} + \ln\left(\frac{\gamma_{MgCr_2O_4}}{\gamma_{FeCr_2O_4}}\right) - \frac{W_{ol}}{RT}$$

$$+ \frac{2W_{ol}}{RT}(X^{ol}_{MgSi_{0.5}O_2}) \quad (21)$$

where $K_a^{ol-Crsp}$ is the equilibrium for the olivine-spinel exchange reaction, $X^{Crsp}_{FeCr_2O_4}$ is the mole fraction of chromite in the spinel solid solution, $\gamma_{FeCr_2O_4} = (a_{FeCr_2O_4}/X^{Crsp}_{FeCr_2O_4})$ is the activity coefficient of chromite in the spinel solid solution, and W_{ol} is the regular solution interaction parameter for Fe-Mg olivine. Predicted $K_d^{ol-Crsp}$ values at fixed spinel composition were calculated from Equation 21 using $\gamma_{FeCr_2O_4}$ and $\gamma_{MgCr_2O_4}$ values from our activity-composition relations. The regular solution interaction parameter (W_{ol}) in olivine was assumed to be 4.5 ± 1.0 kJ/mol on a 1 atom basis (Nafziger and Muan, 1967; O'Neill and Wall, 1987) and the mean value for ln $K_a^{ol-Crsp}$ was calculated to be 3.0. Predicted ln $K_d^{ol-Crsp}$ values at 700 °C are in good agreement with experimental measurements at 700 °C and 800 °C (Fig. 12). Three data points at 900 °C are, however, inconsistent with the lower temperature results and would require a much smaller value of the $g_{r_1r_1}$ coefficient. The $g_{r_1r_1}$ coefficient is given by $-W_{[4]Fe^{2+}-[4]Mg^{2+}}$ (Appendix 1) and our value of −10.0 ± 1.0 kJ/mol is in good agreement with a recent estimate of approximately 8.2 kJ/mol for $W^{spinel}_{Fe^{2+}-Mg^{2+}}$ (Sack and Ghiorso, 1989). The three anomalous data points at 900 °C are therefore, in the context of our model, inconsistent with a wide range of activity-composition, as well as partitioning data summarized in our earlier paper (Jamieson and Roeder, 1984; Lehmann and Roux, 1986; Shishkov et al., 1980; and Trinel-Dufour and Perrot, 1977 summarized in Nell and Wood, 1989).

Data points at the intersection of the $FeCr_2O_4$-$MgAl_2O_4$ and $MgCr_2O_4$-$FeAl_2O_4$ tie lines were used to constrain the value of the $g_{r_1r_3}$ parameter by formulating equilibria similar to Equation 21 for the $FeCr_2O_4$-$MgCr_2O_4$ and $MgAl_2O_4$-$FeAl_2O_4$ components in equilibrium with olivine. Our model calculates equal ratios for ln $\frac{\gamma_{MgAl_2O_4}}{\gamma_{FeAl_2O_4}}$ and ln $\frac{\gamma_{MgCr_2O_4}}{\gamma_{FeCr_2O_4}}$, but the data are poorly reversed and do not provide a stringent test for our model.

Fe_3O_4-$FeCr_2O_4$ solid solutions

Calculated cation distributions at 1400 °C (Fig. 8A) agree with our results obtained from thermopower measurements. Activity-composition relations calculated at 1227 °C are shown in Figure 8B together with the data of Katsura et al. (1975) and Petric and Jacob (1982a). Uncertainties in the latter data were estimated from the experimental method in which spinel solid solutions and Pt-Fe alloys were equilibrated at a fixed P_{O_2}. The uncertainty in the value of log a_{Fe} is approximately ±0.06 log units (Nell and Wood, 1989) resulting in the error bars presented in Figure 8B.

Fe_3O_4-$MgCr_2O_4$ and Fe_3O_4-$FeAl_2O_4$-$FeCr_2O_4$ solid solutions

Cation distributions in Fe_3O_4-$MgCr_2O_4$ solid solutions calculated at 1000 °C are compared with measured values in Figure 9. Measured and calculated cation distributions in Fe_3O_4-$FeAl_2O_4$-$FeCr_2O_4$ solid solutions along a pseudobinary section with the ratio of $Cr_2O_3/(Cr_2O_3 + Al_2O_3) = 1/2$ at 1100 °C are in Figure 10. Data in this system were collected along three pseudobinary sections taken at constant ratios of $FeAl_2O_4/(FeAl_2O_4 + FeCr_2O_4) = 1/6$, 1/1, and 5/6, respectively. This was done to facilitate integration of a three-component Gibbs-Duhem equation (Darken, 1950) for the excess partial molar entropy of Fe_3O_4 in solution that in turn was used to calculate partial molar entropies and cation distributions in $FeAl_2O_4$-$FeCr_2O_4$ solid solutions (Fig. 11A). Uncertainties in the cation distributions obtained from the Gibbs-Duhem integration were estimated in our previous paper (Nell and Wood, 1989) and are indicated on Figure 11A. In situ high-temperature cation distributions in solid solutions that do not contain both Fe^{2+} and Fe^{3+} (e.g., $FeCr_2O_4$-$FeAl_2O_4$) are not amenable to direct measurement using the thermopower-conductivity technique, and this provides a feasible, if ponderous, way of obtaining high-temperature cation distributions in such systems.

Activity-composition relations modeled for $FeCr_2O_4$-$FeAl_2O_4$ solid solutions at 1100 °C are compared to the measurements of Petric and Jacob (1982b) in Figure 11B. Error bars on the data points correspond to an uncertainty of ±10% in the measured activities.

$MgAl_2O_4$-$MgCr_2O_4$ solid solutions

Al^{3+}-Cr^{3+} partitioning experiments between spinel and clinopyroxene at 1100 °C and 25 kbar pressure (Webb and Wood, 1986) were used to constrain activity-composition relations in $MgAl_2O_4$-$MgCr_2O_4$ solid solutions. Assuming ideal mixing in clinopyroxene solid solutions, equilibrium between $NaAlSi_2O_6$-$NaCrSi_2O_6$ (cpx) and $MgAl_2O_4$-$MgCr_2O_4$ (CrAlsp) is given by

$$\ln K_d^{cpx-CrAlsp} = \ln \frac{(X^{CrAlsp}_{MgCr_2O_4})(X^{cpx}_{NaAlSi_2O_6})}{(X^{CrAlsp}_{MgAl_2O_4})(X^{cpx}_{NaCrSi_2O_6})}$$

$$= \ln K_a^{cpx-CrAlsp} + \frac{\ln}{2}\left(\frac{\gamma_{MgAl_2O_4}}{\gamma_{MgCr_2O_4}}\right). \quad (22)$$

Theoretical ln $K_d^{cpx-CrAlsp}$ values at fixed spinel compositions were calculated from our activity-composition re-

lations at 1100 °C and the results are shown in Figure 13A together with the data of Webb and Wood (1986). The mean value of $K_a^{cpx-CrAlsp}$ was found to be 1.05.

The model was also used to predict Cr^{3+}-Al^{3+} partitioning behavior between $MgAl_2O_4$-$MgCr_2O_4$ and Al_2O_3-Cr_2O_3 solid solutions. Oka et al. (1984) crystallized Cr-Al gels and reported partitioning data for this system based on their synthesis experiments at 1250, 1050, and 796 °C at 25 kbar pressure. Equilibrium between asymmetric sesquioxide solid solutions (cor) and symmetric $MgAl_2O_4$-$MgCr_2O_4$ solid solutions (CrAlsp) is given by the following relationship:

$$\ln K_d^{cor-CrAlsp} = \ln \frac{(X^{CrAlsp}_{MgCr_2O_4})(X^{cor}_{Al_2O_3})}{(X^{CrAlsp}_{MgAl_2O_4})(X^{cor}_{Cr_2O_3})} = \ln K_a^{cor-CrAlsp} + \frac{\ln\left(\frac{\gamma_{MgAl_2O_4}}{\gamma_{MgCr_2O_4}}\right)}{2} + \frac{3(W^{cor}_{Cr_2O_3} - W^{cor}_{Al_2O_3})}{2RT}(X^{cor}_{Al_2O_3})^2 + \frac{(4W^{cor}_{Al_2O_3} - 2W^{cor}_{Cr_2O_3})}{2RT}X^{cor}_{Al_2O_3} - \frac{W^{cor}_{Al_2O_3}}{2RT} \quad (23)$$

where $W^{cor}_{Al_2O_3}$ and $W^{cor}_{Cr_2O_3}$ are asymmetric interaction parameters in Al_2O_3-Cr_2O_3 solid solutions. We calculated ln $K_d^{cor-CrAlsp}$ values following the approach outlined above for $FeCr_2O_4$-$MgCr_2O_4$ solid solutions. $W^{cor}_{Al_2O_3}$ and $W^{cor}_{Cr_2O_3}$ values were obtained from Jacob (1978) and Chatterjee et al. (1982) while $K_a^{cor-CrAlsp}$ was set to zero. Our predicted partition coefficients at 1050 °C are in good agreement with data from Oka et al. (1984) at 1050 °C and 1250 °C given the range of possible values for the asymmetric interaction parameters in the sesquioxide (Fig. 13B).

Conclusions

We have presented a large body of thermopower and electrical conductivity data on spinel in the systems Fe_3O_4-$FeCr_2O_4$, and Fe_3O_4-$MgCr_2O_4$ and the ternary Fe_3O_4-$FeAl_2O_4$-$FeCr_2O_4$. From both experimental data and theoretical calculations we have argued that most of the data are consistent with octahedral site electron hopping between Fe^{2+} and Fe^{3+} analogous to that which is observed in pure Fe_3O_4. Activation energies for conduction increase slowly and monotonically away from Fe_3O_4, and cation distributions calculated from the data are consistent with the formalism of O'Neill and Navrotsky (1983, 1984), which is a good description of unary and binary spinels. On the Fe_3O_4-$FeCr_2O_4$ join, we were able to conduct an independent test of the Fe^{2+}-Fe^{3+} hopping mechanism and found agreement between calculated and nominal concentrations of Fe at $FeCr_2O_4$ contents between 0 and 60%. More Cr-rich compositions cannot, however, be described by this conduction mechanism, and we believe it likely that Cr^{3+} is involved at more dilute concentrations of Fe_3O_4.

We used the data to calculate octahedral-tetrahedral cation distributions for these compositions where octahedral Fe^{2+}-Fe^{3+} electron hopping appears to hold. The cation distribution data were then combined with activity-composition relations and interphase partitioning data for chrome-bearing spinels in a model that extends our previous work in $(Mg^{2+},Fe^{2+})(Fe^{3+},Al^{3+})_2O_4$ solid solutions (Nell and Wood, 1989) to the geologically important system $(Mg^{2+},Fe^{2+})(Fe^{3+},Al^{3+},Cr^{3+})_2O_4$. We used a second-degree Taylor series expansion of the vibrational part of the Gibbs free energy in terms of order and composition parameters and constrained the values of the series expansion coefficients to be consistent with cation distribution data, activity-composition relations, and element partitioning data. The model reproduces the data from which the values of coefficients were obtained and also successfully predicts data that were not used to constrain the fit parameters.

A computer program in Fortran 77 has been written to calculate cation distributions and activities in the $(Mg^{2+},Fe^{2+})(Fe^{3+},Al^{3+},Cr^{3+})_2O_4$ system. It is available on diskette or tape from the second author.

Acknowledgments

The paper benefited greatly from constructive reviews by A. Navrotsky, M. Ghiorso, J.M. Honig, and D.M. Sherman. We also appreciate the remarks by H. Schmalzried. The research was made possible in part by financial support from the Council for Mineral Technology (MINTEK) to J.N. Support by NSF Grant EAR-8416793 to B.J.W. is also acknowledged.

References cited

Amthauer, G., and Rossman, G.R. (1984) Mixed valence of iron in minerals with cation clusters. Physics and Chemistry of Minerals, 11, 37–51.

Aragon, R., and Honig, J.M. (1988) Mean-field model for the Verwey transition in magnetite. Physical Review B, 37, 209–218.

Aragon, R., and McCallister, R.H. (1982) Phase and point defect equilibria in the titanomagnetite solid solution. Physics and Chemistry of Minerals, 8, 112–120.

Austin, I.G., and Mott, N.F. (1969) Polarons in crystalline and non-crystalline materials. Advances in Physics, 18, 41–108.

Bannerjee, S.K., O'Reilly, W., Gibb, T.C., and Greenwood, N.N. (1967) The behaviour of ferrous ions in iron-titanium spinels. Journal of Physical Chemistry of Solids, 28, 1323–1335.

Bevington, P.R. (1969) Data reduction and error analysis for the physical sciences, 336 p. McGraw-Hill, New York.

Buddington, A.F., and Lindsley, D.H. (1964) Iron-titanium oxide minerals and their synthetic equivalents. Journal of Petrology, 5, 310–357.

Chaikin, P.M., and Beni, G. (1976) Thermopower in the correlated hopping regime. Physical Review B, 13, 647–651.

Chakraverty, B.K. (1980) Charge ordering in Fe_3O_4, Ti_4O_7 and bipolarons. Philosophical Magazine B, 42, 473–478.

Chatterjee, N.D., Leistner, H., Tehart, L., Abraham, K., and Klaska, R. (1982) Thermodynamic mixing properties of corundum-eskolaite, α-$(Al,Cr^{3+})_2O_3$, crystalline solutions at high temperatures and pressures. American Mineralogist, 67, 725–735.

Darken, L.S. (1950) Application of the Gibbs-Duhem equation to ternary and multicomponent systems. Journal of the American Chemical Society, 72, 2909–2914.

Dieckmann, R. (1982) Defects and cation diffusion in magnetite (IV):

Non-stoichiometry and point defect structure of magnetite ($Fe_{3-\delta}O_4$). Berichte Bunsengesellschaft Physikalische Chemie, 86, 112–118.

Dieckmann, R., Witt, C.A., and Mason, T.O. (1983) Defects and cation diffusion in magnetite (V): Electrical conduction, cation distribution and point defects in magnetite ($Fe_{3-\delta}O_4$). Berichte Bunsengesellschaft Physikalische Chemie, 87, 495–503.

Emin, D. (1975) Thermoelectric power due to electronic hopping motion. Physical Review Letters, 35, 882–885.

Engi, M. (1983) Equilibria involving Al-Cr spinel: MgFe exchange with olivine. Experiments, thermodynamic analysis, and consequences for geothermometry. American Journal of Science, 283-A, 29–71.

Erickson, D.S., and Mason, T.O. (1985) Nonstoichiometry, cation distributions, and electrical properties in Fe_3O_4-$CoFe_2O_4$ at high temperature. Journal of Solid State Chemistry, 59, 42–53.

Gerald, C.F., and Wheatley, P.O. (1984) Applied numerical analysis, 579 p. Addison-Wesley, Reading, Massachusetts.

Ghose, S. (1988) Charge localization and associated crystallographic and magnetic phase transitions in ilvaite, a mixed-valence iron silicate. In S.K. Saxena, Ed., Advances in physical geochemistry, vol. 7, p. 141–161. Springer Verlag, New York.

Gillot, B., Ferriot, J.F., and Rousset, A. (1976) Electrical conductivity of magnetites substituted for aluminium and chromium. Journal of Physical Chemistry of Solids, 37, 857–862 (in French).

Goodenough, J.B. (1980) The Verwey transition revisited. In D.B. Brown, Ed., Mixed-valence compounds, p. 413–425. D. Reidel, Dordrecht.

Grønvold, F., and Sveen, A. (1974) Heat capacity and thermodynamic properties of synthetic magnetite (Fe_3O_4) from 300 to 1050 K. Ferrimagnetic transition and zero-point entropy. Journal of Chemical Thermodynamics, 6, 859–872.

Holstein, T. (1959) Studies of polaron motion Part II. The "small" polaron. Annals of Physics, 8, 343–389.

Ihle, D., and Lorenz, B. (1986) Small-polaron conduction and short-range order in Fe_3O_4. Journal of Physics C: Solid State Physics, 19, 5239–5251.

Irvine, T.N. (1965) Chromian spinel as a petrogenetic indicator. Part 1. Theory. Canadian Journal of Earth Science, 2, 648–672.

Jacob, K.T. (1978) Electrochemical determination of activities in Cr_2O_3-Al_2O_3 solid solutions. Journal of the Electrochemical Society, 125, 175–179.

Jamieson, H.E., and Roeder, P.L. (1984) The distribution of Mg-Fe^{2+} between olivine and spinel at 1300 °C. American Mineralogist, 69, 283–291.

Katsura, T., Wakihara, M., Hara, S., and Sugihara, T. (1975) Some thermodynamic properties in spinel solid solutions with the Fe_3O_4 component. Journal of Solid State Chemistry, 13, 107–113.

Kuipers, A.J.M., and Brabers, V.A.M. (1979) Electrical transport in magnetite near the Verwey transition. Physical Review B, 20, 594–600.

Kündig, W., and Hargrove, R.S. (1969) Electron hopping in magnetite. Solid State Communications, 7, 223–227.

Lehmann, J., and Roux, J. (1986) Experimental and theoretical study of $(Fe^{2+},Mg)(Al,Fe^{3+})_2O_4$ spinels: Activity-composition relationships, miscibility gaps, vacancy contents. Geochimica et Cosmochimica Acta, 50, 1765–1783.

Lotgering, F.K., and Van Diepen, A.M. (1977) Electron exchange between Fe^{2+} and Fe^{3+} ions on octahedral sites in spinels studied by means of paramagnetic Mössbauer spectra and susceptibility measurements. Journal of Physical Chemistry of Solids, 38, 565–572.

Mason, T.O. (1987) Cation intersite distributions in iron-bearing minerals via electrical conductivity/seebeck effect. Physics and Chemistry of Minerals, 14, 156–162.

Mason, T.O., and Bowen, H.K. (1981) Electronic conduction and thermopower of magnetite and iron-aluminate spinels. American Ceramic Society Journal, 64, 237–242.

Mattioli, G.S., and Wood, B.J. (1988) Magnetite activities across the $MgAl_2O_4$-Fe_3O_4 spinel join, with application to the thermobarometric estimates of upper mantle oxygen fugacity. Contributions to Mineralogy and Petrology, 98, 148–162.

Nafziger, R.H., and Muan, A. (1967) Equilibrium phase compositions and thermodynamic properties of olivines and pyroxenes in the system MgO-"FeO"-SiO_2. American Mineralogist, 52, 1364–1385.

Nell, J., and Wood, B.J. (1989) Thermodynamic properties in a multicomponent solid solution involving cation disorder: Fe_3O_4-$MgFe_2O_4$-$FeAl_2O_4$-$MgAl_2O_4$ spinels. American Mineralogist, 74, 1000–1015.

Nell, J., Wood, B.J., and Mason, T.O. (1989) High-temperature cation distributions in Fe_3O_4-$MgFe_2O_4$-$FeAl_2O_4$-$MgAl_2O_4$ spinels from thermopower and conductivity measurements. American Mineralogist, 74, 339–351.

Oka, Y., Steinke, P., and Chatterjee, N.D. (1984) Thermodynamic mixing properties of $Mg(Al,Cr)_2O_4$ spinel crystalline solution at high temperatures and pressures. Contributions to Mineralogy and Petrology, 87, 196–204.

O'Neill, H.St.C., and Navrotsky, A. (1983) Simple spinels: Crystallographic parameters, cation radii, lattice energies, and cation distribution. American Mineralogist, 68, 181–194.

——— (1984) Cation distribution and thermodynamic properties of binary spinel solid solutions. American Mineralogist, 69, 733–753.

O'Neill, H.St.C., and Wall, V.J. (1987) The olivine-orthopyroxene-spinel oxygen geobarometer, the nickel precipitation curve, and the oxygen fugacity of the earth's upper mantle. Journal of Petrology, 70, 59–70.

Petric, A., and Jacob, K.T. (1982a) Thermodynamic properties of Fe_3O_4-FeV_2O_4 and Fe_3O_4-$FeCr_2O_4$ spinel solid solutions. Journal of the American Ceramic Society, 65, 117–123.

——— (1982b) Inter- and intra-crystalline ion-exchange equilibria in the system Fe-Cr-Al-O. Solid State Ionics, 6, 47–56.

Sack, R.O. (1982) Spinels as petrogenetic indicators: Activity-composition relations at low pressure. Contributions to Mineralogy and Petrology, 71, 169–186.

Sack, R.O., and Ghiorso, M.S. (1989) Importance of consideration of mixing properties in establishing an internally consistent thermodynamic database: Thermochemistry of minerals in the system Mg_2SiO_4-Fe_2SiO_4-SiO_2. Contributions to Mineralogy and Petrology, 102, 41–68.

Sherman, D.M. (1987) Molecular orbital (SCF-Xα-SW) theory of metal-metal charge transfer processes in minerals I. Application to $Fe^{2+} \rightarrow Fe^{3+}$ charge transfer and "electron delocalization" in mixed-valence iron oxides and silicates. Physics and Chemistry of Minerals, 14, 355–363.

Shishkov, V.I., Lykasov, A.A., and Il'ina, A.F. (1980) Activity of the components of iron-magnesium spinel. Russian Journal of Physical Chemistry, 54, 440–441.

Tannhauser, D.S. (1962) Conductivity in iron oxides. Journal of Physics and Chemistry of Solids, 23, 25–34.

Thompson, J.B., Jr. (1969) Chemical reactions in crystals. American Mineralogist, 54, 341–375.

Trinel-Dufour, M.C., and Perrot, P. (1977) Thermodynamic study of solid solutions in the system Fe-Mg-O. Annale Chimie, 2, 309–318 (in French).

Tuller, H.L., and Nowick, A.S. (1977) Small polaron electron transport in reduced CeO_2 single crystals. Journal of Physical Chemistry of Solids, 38, 859–867.

Verwey, E.J., Haayman, P.W., and Romeijn, F.C. (1947) Physical properties and cation arrangement of oxides with spinel structures II. Electronic conductivity. Journal of Chemical Physics, 15, 181–187.

Webb, S.A.C., and Wood, B.J. (1986) Spinel-pyroxene-garnet relationships and their dependence on Cr/Al ratio. Contributions to Mineralogy and Petrology, 92, 471–480.

Wu, C.C., and Mason, T.O. (1981) Thermopower measurement of cation distribution in magnetite. American Ceramic Society Journal, 64, 520–522.

Manuscript received June 12, 1989
Manuscript accepted December 21, 1990

Appendix 1.

Thermodynamic coefficients in a second-degree Taylor series expansion for the vibrational part of the Gibbs free energy of Fe_3O_4-$MgFe_2O_4$-$FeAl_2O_4$-$MgAl_2O_4$-$FeCr_2O_4$-$MgCr_2O_4$ solid solutions.

$$g_0 = \mu_4^0 + \mu_7^0 - \mu_3^0 + W_{[4]Mg-[4]Fe^{3+}} - W_{[4]Mg-[4]Fe^{2+}} - W_{[4]Fe^{2+}-[4]Fe^{3+}} + \Delta G_{47}^0 - \Delta G_{34}^0$$

$$g_{r_1} = \mu_3^0 - \mu_8^0 + 2W_{[4]Mg-[4]Fe^{2+}} + W_{[4]Fe^{2+}-[4]Fe^{3+}} - W_{[4]Mg-[4]Fe^{3+}} + \Delta G_{34}^0 - \Delta G_{47}^0$$

$$g_{r_2} = \mu_6^0 - \mu_4^0 + W_{[4]Mg-[4]Al} + W_{[4]Al-[4]Fe^{3+}} + W_{[4]Fe^{2+}-[4]Fe^{3+}} - W_{[4]Mg-[4]Fe^{3+}} - W_{[4]Al-[4]Fe^{2+}} + \frac{W_{[6]Al-[6]Fe^{3+}}}{2} + \Delta G_{28}^0$$

$$g_{r_3} = \mu_9^0 - \mu_4^0 + 2W_{[4]Fe^{2+}-[4]Fe^{3+}} + W_{[4]Mg-[4]Fe^{2+}} - W_{[4]Mg-[4]Fe^{3+}} + W_{[6]Fe^{2+}-[6]Cr} + W_{[6]Fe^{3+}-[6]Cr} - \frac{W_{[6]Fe^{2+}-[6]Fe^{3+}}}{2} + \Delta G_{57}^0 + \Delta G_{34}^0 + \Delta G_{19}^0 + \Delta G_{49}^0 - \Delta G_{47}^0$$

$$g_{s_1} = \mu_5^0 - \mu_6^0 + W_{[4]Fe^{2+}-[4]Fe^{3+}} + W_{[4]Mg-[4]Fe^{2+}} + W_{[4]Al-[4]Fe^{2+}} - W_{[4]Mg-[4]Al} - W_{[4]Al-[4]Fe^{3+}} + W_{[6]Al-[6]Fe^{2+}} + \frac{W_{[6]Al-[6]Fe^{3+}} - W_{[6]Fe^{2+}-[6]Fe^{3+}}}{2} + \Delta G_{56}^0 + \Delta G_{45}^0 - \Delta G_{16}^0 - \Delta G_{28}^0$$

$$g_{s_2} = \mu_3^0 - \mu_4^0 + 2W_{[4]Fe^{2+}-[4]Fe^{3+}} + W_{[4]Mg-[4]Fe^{2+}} - W_{[4]Mg-[4]Fe^{3+}} + \frac{W_{[6]Fe^{2+}-[6]Fe^{3+}}}{2} + 2\Delta G_{34}^0 - \Delta G_{47}^0$$

$$g_{s_3} = \mu_3^0 - \mu_4^0 + 2W_{[4]Mg-[4]Fe^{2+}} + W_{[4]Fe^{2+}-[4]Fe^{3+}} - W_{[4]Mg-[4]Fe^{3+}} + \frac{W_{[6]Mg-[6]Fe^{2+}}}{2} + \Delta G_{34}^0 + \Delta G_{12}^0 - \Delta G_{47}^0 - \Delta G_{16}^0$$

$$g_{r_1r_1} = -W_{[4]Mg-[4]Fe^{2+}}$$

$$g_{r_2r_2} = -W_{[4]Al-[4]Fe^{3+}} - \frac{W_{[6]Al-[6]Fe^{3+}}}{2} - \Delta G_{28}^0$$

$$g_{r_3r_3} = -W_{[4]Fe^{2+}-[4]Fe^{3+}} - W_{[6]Fe^{2+}-[6]Cr} - W_{[6]Fe^{3+}-[6]Cr} + \frac{W_{[6]Fe^{2+}-[6]Fe^{3+}}}{2} - \Delta G_{49}^0$$

$$g_{s_1s_1} = -W_{[4]Al-[4]Fe^{2+}} - \frac{W_{[6]Al-[6]Fe^{2+}}}{2} - \Delta G_{56}^0$$

$$g_{s_2s_2} = -W_{[4]Fe^{2+}-[4]Fe^{3+}} - \frac{W_{[6]Fe^{2+}-[6]Fe^{3+}}}{2} - \Delta G_{34}^0$$

$$g_{s_3s_3} = W_{[4]Mg-[4]Fe^{2+}} - \frac{W_{[6]Mg-[6]Fe^{2+}}}{2} + \Delta G_{16}^0 - \Delta G_{12}^0$$

$$g_{r_1r_2} = W_{[4]Al-[4]Fe^{2+}} + W_{[4]Mg-[4]Fe^{3+}} - W_{[4]Mg-[4]Al} - W_{[4]Fe^{2+}-[4]Fe^{3+}}$$

$$g_{r_1r_3} = W_{[4]Mg-[4]Fe^{3+}} - W_{[4]Mg-[4]Fe^{2+}} - W_{[4]Fe^{2+}-[4]Fe^{3+}} + \Delta G_{47}^0 - \Delta G_{57}^0 - \Delta G_{34}^0 - \Delta G_{19}^0$$

$$g_{r_1s_1} = W_{[4]Mg-[4]Al} - W_{[4]Mg-[4]Fe^{2+}} - W_{[4]Al-[4]Fe^{2+}} + \Delta G_{16}^0 - \Delta G_{56}^0$$

$$g_{r_1s_2} = W_{[4]Mg-[4]Fe^{3+}} - W_{[4]Mg-[4]Fe^{2+}} - W_{[4]Fe^{2+}-[4]Fe^{3+}} + \Delta G_{47}^0 - \Delta G_{34}^0$$

$$g_{r_1s_3} = -2W_{[4]Mg-[4]Fe^{2+}} + \Delta G_{24}^0 + \Delta G_{16}^0 - \Delta G_{12}^0 - \Delta G_{46}^0$$

$$g_{r_2r_3} = W_{[4]Al-[4]Fe^{2+}} - W_{[4]Al-[4]Fe^{3+}} - W_{[4]Fe^{2+}-[4]Fe^{3+}} + W_{[6]Cr-[6]Al} - W_{[6]Fe^{3+}-[6]Cr} + \frac{W_{[6]Fe^{2+}-[6]Fe^{3+}} - W_{[6]Al-[6]Fe^{3+}} - W_{[6]Al-[6]Fe^{2+}}}{2} + \Delta G_{34}^0 + \Delta G_{57}^0 + \Delta G_{610}^0 + \Delta G_{19}^0 - \Delta G_{28}^0 - \Delta G_{47}^0 - \Delta G_{49}^0$$

$$g_{r_2s_1} = W_{[4]Al-[4]Fe^{3+}} + W_{[4]Al-[4]Fe^{2+}} - W_{[4]Fe^{2+}-[4]Fe^{3+}} + \frac{W_{[6]Fe^{2+}-[6]Fe^{3+}} - W_{[6]Al-[6]Fe^{2+}} - W_{[6]Al-[6]Fe^{3+}}}{2} + \Delta G_{28}^0 + \Delta G_{56}^0 - \Delta G_{45}^0$$

$$g_{r_2s_2} = W_{[4]Al-[4]Fe^{2+}} - W_{[4]Al-[4]Fe^{3+}} - W_{[4]Fe^{2+}-[4]Fe^{3+}} + \frac{W_{[6]Fe^{2+}-[6]Fe^{3+}} + W_{[6]Al-[6]Fe^{3+}} - W_{[6]Al-[6]Fe^{2+}}}{2} + \Delta G_{36}^0 - \Delta G_{28}^0 - \Delta G_{34}^0$$

$$g_{r_2s_3} = W_{[4]Al-[4]Fe^{2+}} + W_{[4]Mg-[4]Fe^{3+}} - W_{[4]Mg-[4]Al} - W_{[4]Fe^{2+}-[4]Fe^{3+}} - \Delta G_{24}^0$$

$$g_{r_3s_1} = W_{[4]Al-[4]Fe^{3+}} - W_{[4]Al-[4]Fe^{2+}} - W_{[4]Fe^{2+}-[4]Fe^{3-}} + W_{[6]Cr-[6]Al} - W_{[6]Fe^{2+}-[6]Cr} + \frac{W_{[6]Fe^{2+}-[6]Fe^{3+}} - W_{[6]Al-[6]Fe^{2+}} - W_{[6]Al-[6]Fe^{3+}}}{2} + \Delta G_{28}^0 + \Delta G_{47}^0 - \Delta G_{45}^0 - \Delta G_{19}^0 - \Delta G_{610}^0 - \Delta G_{34}^0 - \Delta G_{57}^0$$

$$g_{r_3s_2} = -2W_{[4]Fe^{2+}-[4]Fe^{3+}} + W_{[6]Fe^{3+}-[6]Cr} - W_{[6]Fe^{2+}-[6]Cr} - \Delta G_{49}^0 - \Delta G_{34}^0$$

$$g_{r_3s_3} = W_{[4]Mg-[4]Fe^{3+}} - W_{[4]Fe^{2+}-[4]Fe^{3+}} - W_{[4]Mg-[4]Fe^{2+}} + W_{[6]Al-[6]Fe^{2+}} + W_{[6]Mg-[6]Cr} - \frac{W_{[6]Mg-[6]Fe^{2+}} - W_{[6]Mg-[6]Al}}{2}$$

$$- W_{[6]Fe^{2+}-[6]Cr} + \Delta G^0_{810} + \Delta G^0_{16} + \Delta G^0_{28} - \Delta G^0_{49} - \Delta G^0_{12} - \Delta G^0_{46}$$

$$g_{s_1s_2} = W_{[4]Al-[4]Fe^{3+}} - W_{[4]Fe^{2+}-[4]Fe^{3+}} - W_{[4]Al-[4]Fe^{2+}} + \frac{W_{[6]Al-[6]Fe^{3+}} - W_{[6]Al-[6]Fe^{2+}} - W_{[6]Fe^{2+}-[6]Fe^{3+}}}{2} + \Delta G^0_{28} - \Delta G^0_{45} - \Delta G^0_{36}$$

$$g_{s_1s_3} = W_{[4]Mg-[4]Al} - W_{[4]Mg-[4]Fe^{2+}} - W_{[4]Al-[4]Fe^{2+}} + \frac{W_{[6]Mg-[6]Fe^{3+}} - W_{[6]Fe^{2+}-[6]Fe^{3+}} - W_{[6]Mg-[6]Fe^{2+}}}{2} + \Delta G^0_{16} - \Delta G^0_{56}$$

$$g_{s_2s_3} = W_{[4]Mg-[4]Fe^{3+}} - W_{[4]Mg-[4]Fe^{2+}} - W_{[4]Fe^{2+}-[4]Fe^{3+}} + \frac{W_{[6]Mg-[6]Al} - W_{[6]Al-[6]Fe^{2+}} - W_{[6]Mg-[6]Fe^{2+}}}{2} + \Delta G^0_{16} + \Delta G^0_{78} - \Delta G^0_{34} - \Delta G^0_{12}$$